LBL-10954

Lawrence Berkeley Laboratory
UNIVERSITY OF CALIFORNIA

Physics, Computer Science & Mathematics Division

EXPERIMENTAL STUDY OF RADIATIVE PION CAPTURE ON ^{13}C, ^{20}Ne, ^{90}Zr, ^{19}F AND ^{12}C

Charles Jeffrey Martoff
(Ph.D. thesis)

November 1980

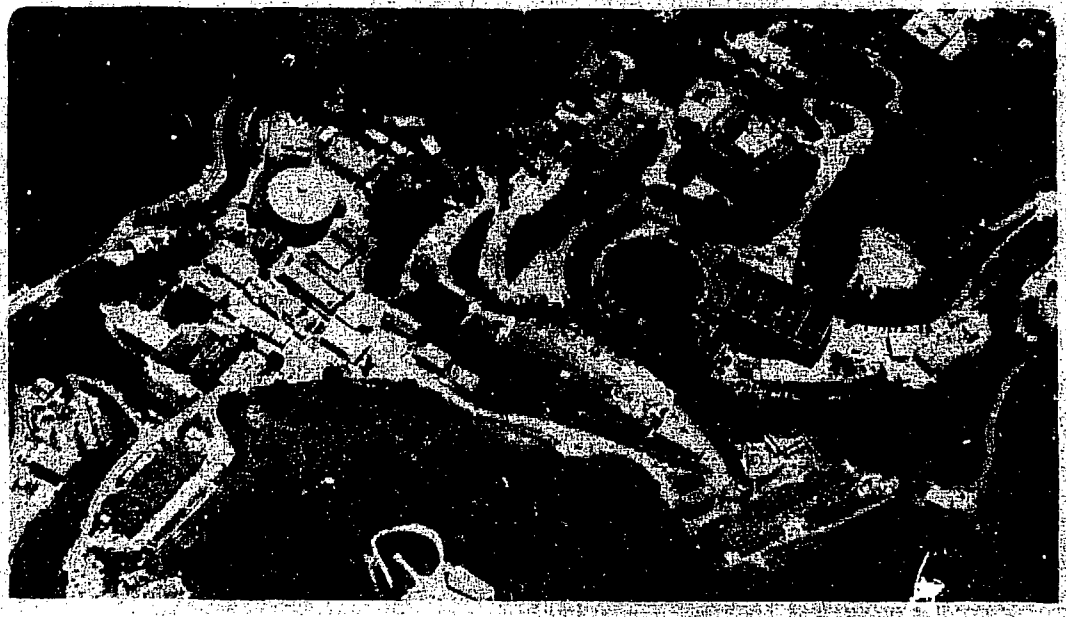

Prepared for the U.S. Department of Energy under Contract W-7405-ENG-48

TABLE OF CONTENTS

EXPERIMENTAL STUDY OF RADIATIVE PION CAPTURE ON ^{13}C, ^{20}Ne, ^{90}Zr, ^{19}F AND ^{12}C

Charles Jeffrey Martoff

Lawrence Berkeley Laboratory
University of California
Berkeley, California 94720

ABSTRACT

Photon spectra for $50 < E_\gamma < 135$ MeV have been measured from the radiative capture of stopped negative pions by the nuclides ^{13}C, ^{19}F, ^{20}Ne, and ^{90}Zr. The e^+e^- pair spectrometer system used has resolution 850 keV FWHM and photon detection efficiency $5 \cdot 10^{-6}$.

The total radiative capture branching ratios measured are: ^{13}C $(1.66 \pm 0.25)\%$, ^{19}F $(2.40 \pm 0.48)\%$, ^{20}Ne $(1.60 \pm 0.24)\%$, and ^{90}Zr $(2.1 \pm 0.5)\%$.

The partial radiative capture branching ratios to four bound states and two resonances in ^{20}F, and two bound states and three resonances in ^{13}B have also been measured.

The branching ratio for $^{13}C(\pi^-,\gamma)^{13}B$ g.s. is $(6.1 \pm 1.2) \cdot 10^{-4}$. Comparison of this result with the beta decay rate of ^{13}B shows that $(84 \pm 16)\%$ of the pion capture amplitude is accounted for by the Gamow-Teller matrix element. Further analysis suggests that much of the

remaining strength is E2.

The measured branching ratios to resonant states in $^{13}C(\pi^-,\gamma)^{13}B$ are shown to be in agreement with detailed shell model calculations of this process. The total single-particle strength in these transitions is shown to be approximately half as large as that of the T = 3/2 part of the E1 photoresonance (the Giant Dipole Resonance) in ^{13}C.

The branching ratio for $^{20}Ne(\pi^-,\gamma)^{20}F$ ($T = 1$, $J^\pi = 1^+$, $E_x = 1.06$ MeV) is $(0.91 \pm 0.52) \cdot 10^{-4}$. Comparison with the electroexcitation of the analog giant M1 state in ^{20}Ne (11.24 MeV) shows that the M1 transition amplitude is less than $(46 \pm 14)\%$ Gamow-Teller. This result is in agreement with detailed shell model calculations of the M1 transition.

The photon spectrum for radiative pion capture from flight (reaction $^{12}C(\pi^+$ T = 44 MeV, γ at 90°)) has been measured. The energy integrated cross section for 0 - 22 MeV excitation of the recoiling ^{12}N is 59 ± 12 μb/sr, in good agreement with published calculations. At higher excitation, evidence for quasifree radiative capture is observed.

I. OVERVIEW OF HISTORY

The radiative capture of stopped $\pi^-[\pi^- + {}^{A}_{N}Z \rightarrow \gamma + {}^{A}_{N+1}(Z-1)]$ was first studied in hydrogen and deuterium, in order to determine the basic properties of the pions and their interaction with nucleons. Panofsky and co-workers[1] in 1951 measured photon spectra, obtained an accurate value for the π^0 mass, and verified the pseudoscalar nature of the pions. They also noted the anomalously large branching ratio for $\pi^- p \rightarrow n\gamma$ compared to $\pi^- p \rightarrow n\pi^0$. This branching ratio has become known as the Panofsky ratio, and its measured value is now 1.543 ± 0.008.[2] Brueckner and co-workers[3] in the same year showed that this branching ratio was consistent with pion photoproduction cross sections.

Early measurements of the total radiative branching ratios for a variety of nuclides were performed in 1965-66 by Davies *et al*[4] and by Petrukhin and Prokoshkin.[5] The total radiative branching ratios were found to be about 2% for nuclides from carbon to lead. Davies *et al* also obtained photon energy spectra. These were not well fitted by simple phase space curves for $\pi^- + {}^{A}_{N}Z \rightarrow \gamma + {}^{A-x}_{N+1-x}(Z-1) + xn$, implying that some nuclear dynamics was important in the process.

Much of the impetus for further work in nuclear capture of pions came from developments in the study of weak interactions by the nuclear capture of negative muons. Early measurements of the total μ^- capture rates seemed to be consistent with the Universal Weak Interaction hypothesis.[6] However, further detailed calculations in a variety of independent-particle nuclear models,[7-9] revealed some persistent disagreements with more refined experiments.[10]

In 1964 Foldy and Walecka suggested[10,11] that the excitation of collective nuclear states could be important in determining the capture rates. The dominant weak interaction terms were shown to be closely related to the electromagnetic operator that excites the El photoresonance. However, the El photoresonance is observed to be shifted upward in energy by 10-15 MeV from independent particle estimates, due to its collective nature.[6] When such final state energy shifts were included in the muon capture calculations, good agreement with the measured capture rates was obtained.[10]

Thereafter, much of the interest in nuclear meson capture centered upon nuclear structure investigations, in particular the observation of novel collective states. Among these were the family of coupled spin and isospin giant resonances proposed as early as 1959 by Glassgold *et al*,[12] by Foldy and Walecka,[13] and by Überall.[14] The El photoresonance (the isospin mode) was the only one of these resonances yet seen experimentally. In 1966 Delorme and Ericson[15] and Anderson and Eisenberg[16] recognized that radiative pion capture would be likely to excite the coupled spin-isospin mode, if it existed. These expectations were based upon the form of the transition operator known from pion photoproduction. Since the (π^-,γ) reaction leading to bound or resonant nuclear states would have a two-body final state, the nuclear excitation energy could be directly measured from the photon energy spectrum. Detailed calculations[17] including the collective effects were done for ^{12}C. Sharp resonant structure in the nuclear excitation spectrum was predicted due to the spin-isospin states. The structure was observed experimentally at LBL in 1970.[18] The interest in these resonances persists to the present day.

The observations in $^{13}C(\pi^-,\gamma)$ are discussed in Section VI.E of the present work.

The pion radiative capture reaction on nuclei has also been used as a test of the CVC and PCAC relations.[19] These relations connect the s-state pion capture matrix elements to those of nuclear beta decay and electron scattering without the introduction of a nuclear model.[20] However, the isolation of the s-state capture has proved to be difficult experimentally and was first achieved only recently,[21] at SIN. The 1s capture rate in ^6Li is within 15% (1.2 standard deviations) of CVC/PCAC predictions. However, the superior agreement obtained in a semi-phenomenological comparison of the 1s capture rate with other available weak and electromagnetic data on ^6Li suggests that there are difficulties in the handling of rho meson exchange and other corrections in the CVC calculation, and not in the understanding of the radiative pion capture process.[21]

The framework developed in these studies led to comparisons between different probes for many transitions, with a specific interest in the nuclear physics content. The extensive measurement nuclides throughout the periodic table carried out by the Berkeley [illegible] have been reviewed.[19] The second-generation experiments at SIN have benefited from the much higher rates at the "meson factory" and have incorporated improvements in the apparatus and different analysis procedures.[22] A review of the nuclear structure information gained from those measurements is in press.[23] The quantitative similarity between strong M1 transitions excited by inelastic electron scattering and the analog transitions seen in radiative pion capture was established in

the work of the LBL and SIN groups over the past decade.

The present work is devoted to the extraction of nuclear structure information from the (π,γ) spectra in combination with other probes. The principal interest lies in the comparison of $\Delta J^{\pi} = 1^{+}$ transitions with allowed Gamow-Teller beta decays and M1 or mixed M1 and E2 inelastic electron scattering to the analog states. The probes are complementary in that matrix elements may be measured or constrained by the combined measurements that are inaccessible in single experiments. At the present level of development, the (π^{-},γ) reaction is seen to be quite useful for obtaining quantitative information on both the usual and unusual features of these transitions.

II. OBJECTIVES AND SUMMARY OF THE PRESENT WORK

The objective of this work is to study the strong M1 and M2 isovector excitations of selected nuclei. To this end, photon spectra from radiative pion capture have been measured. The pion capture transitions to individual final states are compared to other transitions involving these states or their analogs.

The M1 transitions are complex enough that no single experiment can measure all the matrix elements involved. To aid in combining information from electroexcitation and beta decays with radiative pion capture, a set of formulae has been collected from the literature and presented here in a consistent notation.

If complete data from all three probes is available, it is possible to measure separately the spin density and orbital current contributions to magnetic transitions. This is because the electroexcitation proceeds through both these contributions, while the pion capture and beta decay do not couple to the orbital current of nucleons. One can thus subject shell model calculations of these transition amplitudes to more stringent experimental tests by including the radiative pion capture data.

^{13}C and ^{20}Ne each have a strong M1 transition, for which electroexcitation data is available. The Gamow-Teller beta decay ft value for ^{13}B has also been measured. All the experimental data on these transitions, including the radiative pion capture measured here, are shown to be consistent. The importance of a spin flip E2 component of the ^{13}C transition is suggested. ^{20}Ne pion capture data combined with electroexcitation provides a nice test of extensive shell model calculations for this M1 transition.[24] An M1 transition density has two parts, one

arising from the magnetization due to nucleon spins and the other arising from the magnetization due to the orbital current of nucleons. The predicted spin density and orbital magnetization density transition matrix elements are each shown to be in agreement with the present experiment.

The detailed study of relatively well understood transitions at the moderate momentum transfers used here is also important groundwork for future studies of exotic phenomena such as pion condensation and nuclear critical opalescence. These phenomena should appear as momentum transfer dependent enhancements in the spin flip transition densities.[25] The comparison of a number of probes will be important in isolating these effects.[26]

The study of radiative pion capture in flight will be necessary if momentum transfer dependent effects in magnetic transitions are to be studied with pion capture. The capture at rest to a particular final state occurs at a fixed momentum transfer, equal to the photon momentum. The capture in flight of pions well below the 3,3 resonance could impart momentum transfers of 2-3 m_π/c, to nucleons deep in the nuclear interior. For example, $^{12}C(\pi\ T = 75\ MeV, \gamma)$ occurs at $q = 2.5\ m_\pi/c$ for photons observed at 135 degrees from the pion beam direction. The potential gain in information from in-flight capture over capture at rest may be likened to the advantages of electroexcitation studies over the observation of electromagnetic decays to the ground state. The increase in experimental difficulty is also substantial, due to the low rates (dictated by the thin targets needed for good energy resolution in a charged particle beam experiment) and the higher photon energies. Some data on the radiative capture in flight of π^+ at 44 MeV were obtained in this work

in order to assess the feasibility of such measurements and make a first comparison with theoretical calculations.[27] The predicted cross section is in agreement with the present experiment in the photon energy region considered in the calculations. The calculations were based on phenomenological matrix elements from electron scattering. The agreement obtained is encouraging for more detailed comparisons of the two probes, but more pion capture data with improved photon energy resolution are required to isolate individual final states.

Strong M2 transitions have been observed in (π^-,γ)[18,28,29] and (e,e') reactions.[30] These transitions have been discussed as bulk oscillations of spin and isospin. Such coupled oscillations have been theoretically predicted.[12-14] Theory predicts a family of giant resonances, including the El photoresonance (the isospin mode), spin waves, and coupled spin-isospin waves, all with similar properties.

The collective enhancement of the T = 3/2 M2 resonances in $^{13}C(\pi^-,\gamma)^{13}B$ is discussed here by comparing their strength to that of the El photoresonance of ^{13}C. It is seen that the strengths in appropriate single particle units are indeed similar, the M2 states being about half as strong as the T = 3/2 part of the photoresonance.

The strong theoretical analogy between the isospin oscillations (the El photoresonance) and the spin-isospin oscillations (the M2 states) persists only if single-particle transitions differing by spin flip (e.g., $p_{1/2} \rightarrow d_{5/2}$ and $p_{3/2} \rightarrow d_{3/2}$) are nearly degenerate.[11,31] The spin-orbit interaction may invalidate this assumption as the nuclear mass increases, partly explaining the apparent absence of M2 resonances in the (π^-,γ) reaction on medium and heavy nuclei.[19] The

fragmentation of the resonances may be enhanced in particular cases by the pairing effect of an additional odd nucleon. This situation exists in ^{19}F when compared to $^{16,18}O$. The strong M2 resonance structure in the (π^-,γ) spectra of the oxygen isotopes yields to a nearly smooth spectrum in the case of $^{19}F(\pi^-,\gamma)^{19}O$. The strength appears spread over a number of low-lying negative parity states in the recoil ^{19}O nucleus.

These studies support the picture of the M2 resonances as collective oscillations of spin and isospin, arising when many nearly degenerate shell-model states are profoundly mixed by a weak residual interaction. This is precisely the mechanism explaining the E1 photoresonance in the context of the shell model.[32]

We have studied the strong M1 transitions in ^{13}C and ^{20}Ne, and the M2 resonances in ^{13}C, ^{20}Ne and ^{19}F. We find that if E2 contributions are included when required, all the weak electromagnetic and pion capture data are mutually consistent and in accord with shell model calculations.

III. EXPERIMENTAL METHOD

The data upon which this work is based was obtained at the Low Energy Pion Channel of the Clinton P. Anderson Meson Physics Facility from Los Alamos Experiment 348, during the summer of 1978.

The apparatus used is an electron-positron pair spectrometer which has been used before, and its properties are described in detail in Ref. 28. A schematic diagram of the set-up appears in Figure 1.

The magnet is a twin-C type with a single common pole tip. The pole area is 218.0 cm by 40.5 cm, with a 33.0 cm gap. The magnetic field used is 8.0 kG.

At the entrance to the magnet are suspended two 3-plane multiwire proportional chambers (MWPCs). The active area of each MWPC is 200 cm by 25 cm, nearly covering the magnet aperture. Each MWPC has sense wires running vertically and at ±30° from the horizontal, with 2 mm spacing between wires. Using three-wire intersections, particle tracks are found without ambiguity. The spatial resolution is nearly equal in the horizontal and vertical directions with this wire arrangement.

Just in front of the chamber nearest the stopping target are the photon converters. A "thick" 0.010 cm gold converter foil is followed by a plastic scintillator and a second "thin" 0.005 cm gold foil. This allows the acquisition of an improved energy resolution data sample by tagging events from the thin converter with the absence of a signal from the scintillator between the foils.

Covering the front of the chambers are two rows of 8 mm thick plastic trigger counters (A B counters numbered 1 through 8). The A B counters and the MWPCs are shielded from charged particles from the beam

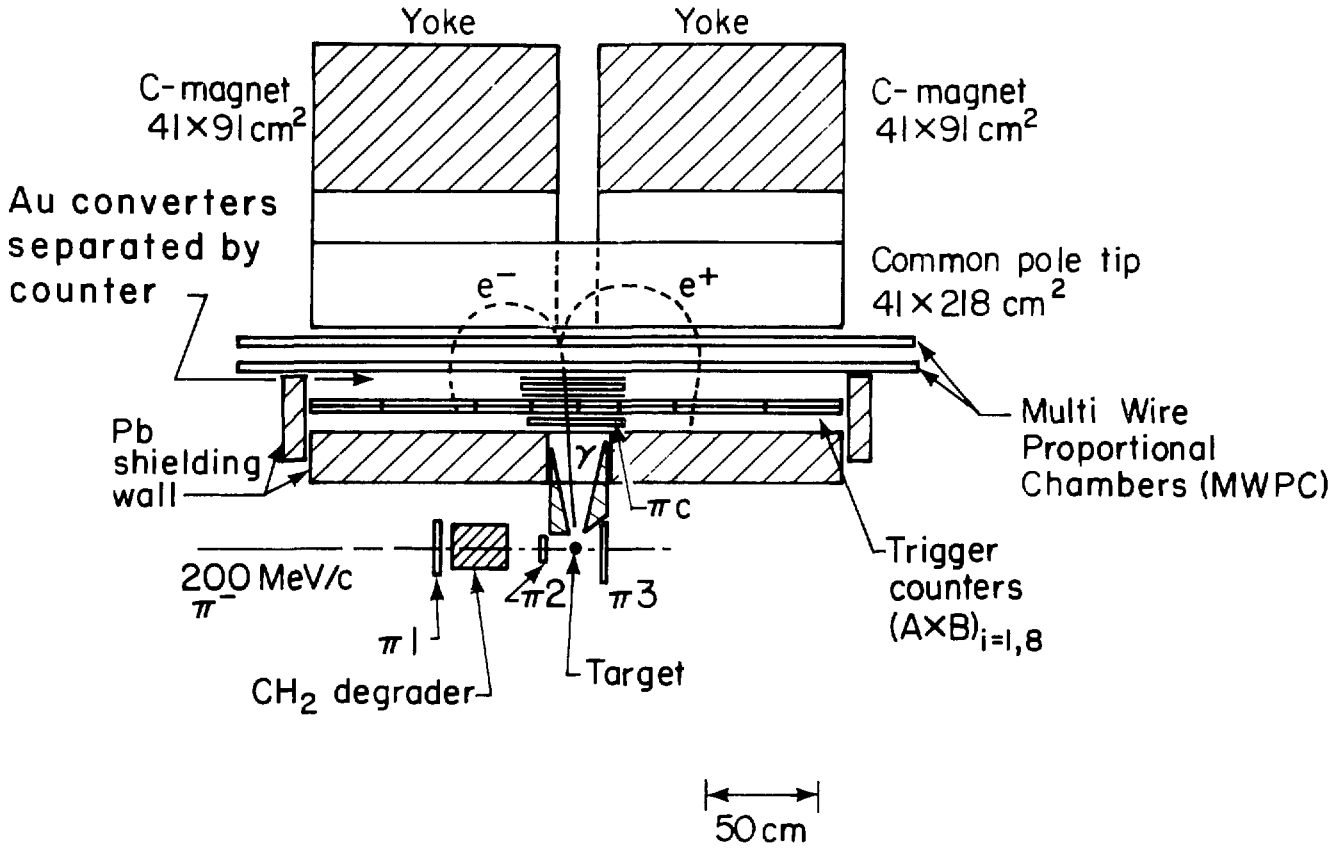

Fig. 1. Schematic diagram of experimental apparatus. XBL 801-16A

and the target by a lead wall 20 cm thick. Photons from the target are admitted through a hole in this lead, which is covered by a plastic scintillator used to discriminate against charged particles.

The event trigger requirement for data taking at high incident pion fluxes includes a coincidence between two nonadjacent pairs of A B counters, fast signals from at least two planes of each MWPC, and no charged particle veto counter pulse. The A B counters detect the e^+e^- pairs from photon conversion as they exit from the magnet. A conventional three-element beam telescope is used for range optimization and for determining the normalization by counting individual beam particles at appropriately reduced beam rates (see Section IV.C).

An event trigger causes the triggering electronics to be gated off, and the chambers to be read out by an LBL CAMAC electronic system[33] to a PDP 11/45 computer using an MBD-11 acquisition system.[34] The chamber information and the reporting trigger counter numbers are stored in the computer memory until a buffer is filled, which is then written to tape. The data acquisition is handled by the Los Alamos standard software system "Q".[35]

The event trigger rate is about 100 per second for a hydrogen target and about 10 per second for other targets. The smaller rate for other targets results from the typical radiative branching ratios of 0.02 compared to 0.39 for hydrogen.

The instantaneous pion fluxes used for data taking were in excess of 10^9 sec^{-1}, preventing flux measurement by individual pion counting. Therefore the following procedure was adopted for each target and for hydrogen. A two-element telescope was set up to count pions backscattered from the degrader at 125^o. This "monitor" remained in place throughout the experiment. The pion channel momentum bite and solid angle can be independently varied by two sets of adjustable slits.[36] First the momentum bite was reduced from the 2% dp/p used for data taking to 0.5%. The intensity slits were also closed until the pion rate was below 10^6 sec^{-1}, and a conventional three-element beam telescope was used to optimize the degrader thickness for maximum π_{STOP}/π_{IN}, target in minus target out. The backscattering monitor was calibrated against the beam telescope as well. Then the intensity slits were opened and sufficient data accumulated for a relative normalization, using the calibrated monitor.

The fraction of incident pions stopping in each target at its optimum degrader thickness, measured during the degrader optimization, was checked by computing the equivalent thickness of the target relative to the hydrogen target. These calculations agreed with the measured stopping fractions to within 7% of π_{STOP}/π_{IN}. These data are given in Appendix A in units of inches of added CH_2 degrader that would have stopped as many pions as the target.

We deduce $\eta_\gamma(E_0) = 4.97 \pm 0.5) \cdot 10^{-6}$ for the overall absolute photon acceptance for the thin converter, and $\eta_\gamma(E_0) = (1.01 \pm 0.1) \cdot 10^{-5}$ for the thick converter from the hydrogen data.

IV. DATA ANALYSIS

A. The Wind-Fit Method for Trajectory Analysis

For the analysis of the pair trajectories, a procedure described by Wind[37] and previously used at the SIN pair spectrometer[22] was implemented. The Wind-Fit method uses simulated particle trajectories to develop interpolation formulae for the momentum and angles of particles in terms of the measured wire chamber crossing coordinates. The procedure is as accurate as iterative least squares fitting of each trajectory, the rms deviation from the true momentum being 100 keV for a set of 1000 simulated trajectories. The Wind-Fit method, however, requires much less computer time for the analysis of data, since the momentum is obtained from an analytic formula rather than an iterative procedure.

To simulate particle trajectories passing through the pair spectrometer, a complete map of all three components of the magnetic field was required. The map was measured on a 1-inch cubic grid.

No multiple scattering or other stochastic processes were included in the simulation because these have been found to degrade the accuracy of the fits obtained.[22] For each trajectory which passed through the spectrometer, the coordinates at which the MWPC planes were crossed were recorded, as well as the particle momentum, incident angles, and conversion position.

Interpolation formulae for the momentum, angles, and conversion position in terms of the MWPC crossing coordinates were then computed by Wind's method.

The accuracy of the interpolation formulae when applied to real

events depends upon the number of simulated trajectories used in the computation. However, the procedure converges quite rapidly in practice. The present 850 keV FWHM thin converter resolutions was obtained from a fit to 364 trajectories. One thousand trajectories were fitted for the thick converter without improving the resolution beyond 1.75 MeV.

B. Event Reconstruction

A computer code has been developed[38] which seeks the pattern of an e^+e^- pair in the MWPC addresses recorded for each data event. The coordinates of the MWPC crossings are paired off into trajectory candidates and tested for the symmetry and incident angles expected for an e^+e^- pair resulting from conversion of a photon from the target in the converter foil. The pair of candidates for electron and positron with the closest origins on the converter according to the Wind-Fit formula is selected from each event.

Twenty-two percent of the event triggers were recognized as pairs and analyzed by this system. Scanning of 360 events by eye showed that 36% had the topology of a pair.

Ten percent of the thin converter events and 30% of the thick converter events analyzed failed cuts imposed on the traceback to the target and the incident angles of the e^+e^-. These cuts eliminate nontarget-associated photons, photons that convert in the lead wall or in the target itself, and events in which the electron or positron underwent a large-angle scattering while entering the spectrometer. The effect of the cuts on the thick converter data is to improve the resolution from 2.2 MeV to 1.75 MeV FWHM. The thin converter cuts

eliminate primarily events outside the resolution width, in the high and low energy "tails" of the lineshape.

Grand total energy histograms for each target were accumulated and in some cases subtraction of appropriate "target empty" spectra was performed. The subtraction amounted to less than 20% of the total number of events in all cases.

The number of event triggers retained after each stage of the analysis is summarized in Table 1 below. The cuts applied to the recognized pairs are given in Table 2.

The photon energy histograms were fitted to sums of sharp lines, Breit-Wigner resonance shapes, and a convenient parametrization of the smooth continuum component. The fitting function included the measured lineshape and acceptance curve of the spectrometer.

The lineshape was taken from observed spectra of the sharp line from capture in hydrogen ($\pi^- p \rightarrow n\gamma$). A background contribution determined from empty dewar runs was subtracted, and the same cuts applied to the

TABLE 1. Event triggers retained after each stage of analysis.

Event triggers on original data tape	100%
At least three groups of wires firing in each MWPC plane	63%
Recognized pairs	22%
Accepted in final histogram,	
thin converter	20%
thick converter	15%
(Apparent pairs found by visual scanning)	(36%)

TABLE 2. Cuts applied to analyzed events.

	Thick Converter	Thin Converter
Horizontal coordinate of photon extrapolated to stopping target	<5.12 cm downstream of target center	<4.5 cm downstream of target center
Horizontal angle between e^+ or e^- trajectory and normal to converter foil	<8.7°	--
Horizontal separation of pair at converter	--	<0.66 cm

data being analyzed were applied to the hydrogen data used for the lineshape. The hydrogen lineshape for the thin converter is shown in Figure 2.

C. Normalization of Branching Ratios

The energy dependence of the pair spectrometer system acceptance was obtained empirically. The spectrum of $^{12}C(\pi^-,\gamma)$ has been measured in Berkeley[28] as well as at SIN.[39] The acceptance curve for the present experiment was constructed by a fit of the ^{12}C spectrum obtained here to the SIN spectrum. The resulting curve is shown in Figure 3. The errors result from the statistics of the ^{12}C data from the present experiment.

The hydrogen spectrum has, in addition to the sharp line at 129.4 MeV from $\pi^-p \to n\gamma$, a low-energy component from $\pi^-p \to n\pi^0$; $\pi^0 \to 2\gamma$, and the ratio of the latter reaction to the $\pi^-p \to n\gamma$ component has been precisely measured. The spectrum of photons from the π^0 decay is a

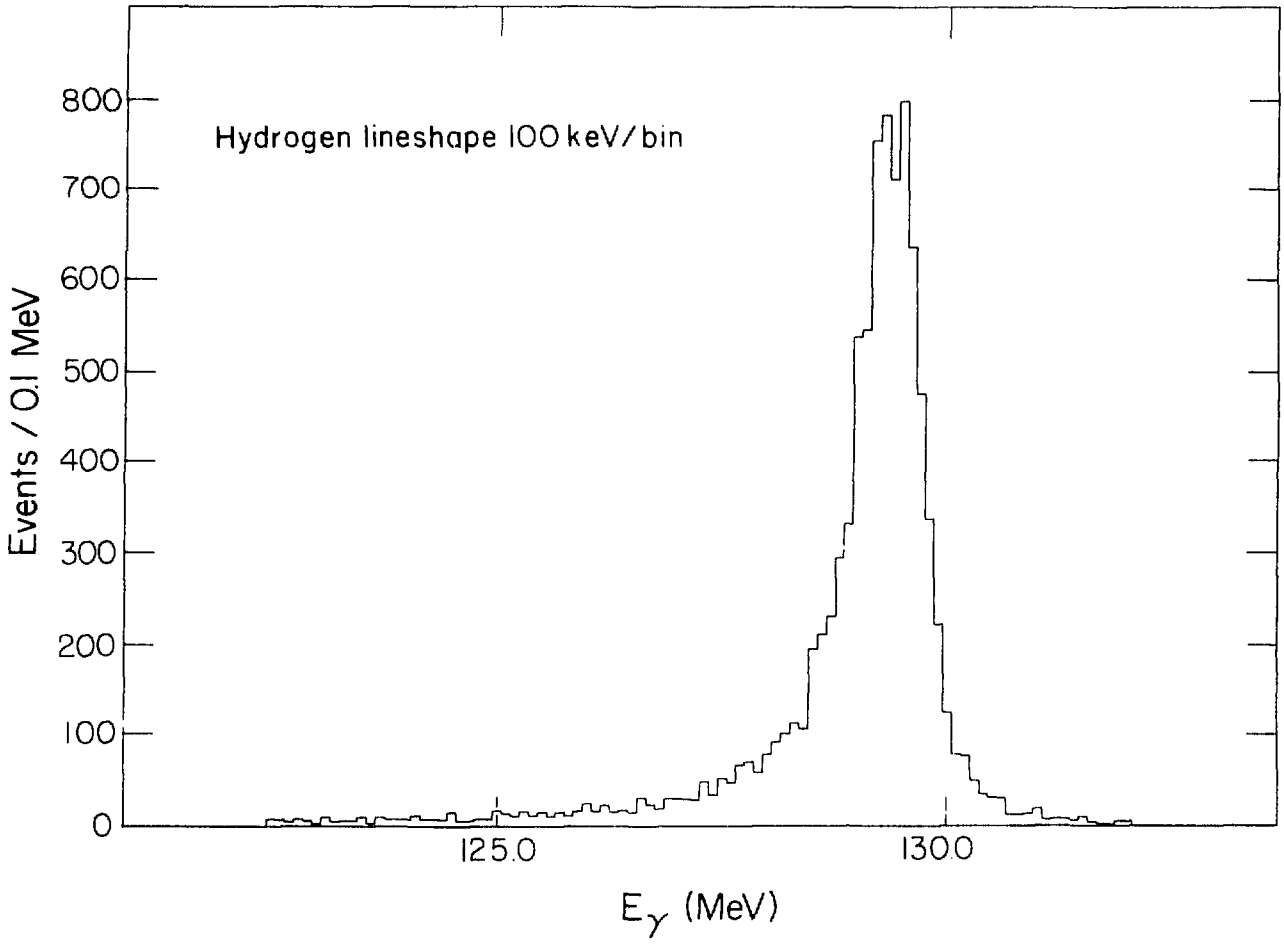

Fig. 2. Spectrometer response function measured with monochromatic 129.4 MeV photons from $\pi^- p \rightarrow n\gamma$. The displayed energy has been corrected for losses in the converter foils and MWPC's.

XBL 806-1227

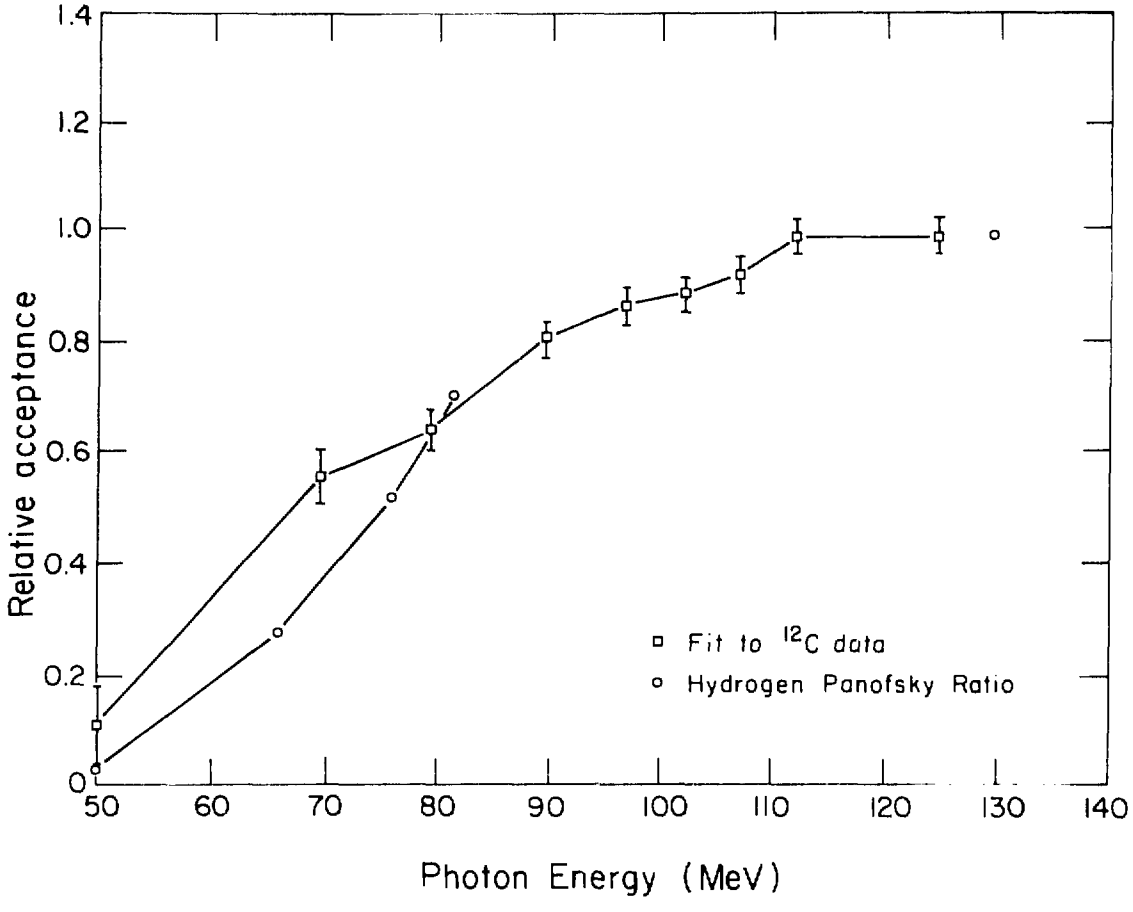

Fig. 3. Acceptance of the pair spectrometer system as a function of photon energy, determined by fits to hydrogen and ^{12}C radiative capture spectra.

XBL 806-1223

square box between 54.8 and 83.0 MeV. After convolving this spectrum with the spectrometer lineshape, a check on the ratio of acceptance at 129.4 MeV to that at low energies was obtained, and this ratio was consistent with the curve constructed from the ^{12}C spectrum.

For comparison, the trajectory-simulating program was used in an attempt to track through the spectrometer a fixed number of pairs having energies between 50 and 150 MeV. The incident angles and conversion positions of these pairs were stepped over the available space on a rectangular lattice. The pairs that passed through the spectrometer were recorded. These pairs were then subjected to the requirements imposed on actual data by the pattern recognition program, by the experimental cuts, and by the geometrical requirements of the trigger. The variation in pair production cross section (20%) occurring between $50 < E_\gamma < 150$ MeV was also taken into account, but the trigger counter and wire chamber efficiencies were not. The resulting histogram is an unnormalized acceptance curve for the spectrometer system. The effects of multiple scattering, which were neglected in this treatment, result in a gradual reduction of acceptance as the photon energy drops. This curve is also shown in Figure 3.

For the determination of absolute branching ratios, we rely upon hydrogen calibration runs and the procedure described in Section III. A formula relating the unknown branching ratio for a given nuclear target to the known hydrogen yield may be obtained as follows.

The number of events H observed in the radiative capture line at E = 129.4 MeV is given by

$$H = \eta_\gamma(E_0)\, R_\gamma^H\, \pi_S^H \quad .$$

In this expression, $\eta_\gamma(E_0)$ is the absolute acceptance of the pair spectrometer system at E_0, R_γ^H is the hydrogen radiative branching ratio, given by $[1/(1+P)] = 0.393 \pm 0.001$, where P is the Panofsky ratio, and π_S^H is the number of pions stopped in the hydrogen target.

Similarly, the number of events in the spectrum of a target T is

$$T = \int \frac{dT}{dE}\, dE = \left(\int \eta_\gamma(E)\, \frac{dR_\gamma^T(E)}{dE}\, dE \right) \pi_S^T \quad .$$

From this one obtains the branching ratio for T in the terms of R^H:

$$\frac{R_\gamma^T}{R_\gamma^H} = \frac{\int \frac{dR_\gamma^T(E)}{dE}\, dE}{\left(\frac{H}{\eta_\gamma(E_0)\pi_S^H} \right)} = \frac{\frac{1}{\pi_S^T} \int \frac{1}{\eta_\gamma(E)}\, \frac{dT}{dE}\, dE}{\left(\frac{H}{\eta_\gamma(E_0)\pi_S^\pi} \right)}$$

$$= \frac{\pi_S^H}{\pi_S^T}\, \frac{T}{H} \left(\frac{1}{T} \int \frac{\eta_\gamma(E_0)}{\eta_\gamma(E)}\, \frac{dT}{dE}\, dE \right) \quad .$$

The factor in large parentheses may be defined as the unfolding factor U. This factor is calculated from the final spectrum and the relative acceptance curve. The value of the unfolding factor depends upon the shape of the target spectrum.

This formula for the branching ratio is given in terms of ratios between data on T and data on hydrogen, cancelling the errors common to both quantities.

D. Measurement Errors in the Branching Ratios

The uncertainties in the measured branching ratios arise from four independent sources:

1) statistical errors in H and T,
2) errors in the ratio π_S^H/π_S^T ,
3) errors in U,
4) errors from the fits to the spectra.

The errors in H and T are evaluated from counting statistics.

The errors in the ratio π_S^H/π_S^T are evaluated by comparing the values measured during range optimization to those calculated from the target thicknesses and stopping powers. For each target, these values agreed to within 7%. The error in the ratio is therefore taken to be $(\sqrt{2})(0.07) = 10\%$.

The errors in U arise from the uncertainty of the acceptance curve, weighted with the measured spectra. The best known parts of the acceptance curve are thereby weighted most heavily. The errors are about 4%. The precise values are shown in Table A-2 of Appendix A.

The fitting errors arise when partial branching ratios to individual final states are evaluated. The branching ratios to individual final states (peaks in the photon energy spectra) were obtained by fitting the spectra with lines and a background as discussed in Section C of this chapter. The fraction of the spectrum contained in the fitted line was multiplied by the total radiative branching ratio to give the partial branching ratio. The precision of the fitted line strengths depends both upon the counting statistics of the peak being fitted and upon the correlation of that peak height with others. Thus the partial branching ratios to isolated peaks may be obtained more accurately than those to peaks lying closer together than the resolution width. Correlation

coefficients and errors for the fitted line strengths are computed in the fitting program. The correlations contribute significantly to the uncertainties when fitted peaks are not completely resolved.

The energy dependence of the acceptance could also contribute an error to the peak heights. This error is smallest when the energy of the peak is close to that of the hydrogen peak used as the acceptance standard, and therefore varies from one peak to another. The acceptance at the energy of each peak is found by linear interpolation between two energies where the acceptance has been evaluated. The errors of these two acceptance values are combined in quadrature with weights given by the interpolation formula to obtain the error of the interpolated value. The result is less than 7% for each of the observed lines. The precise value for each line has been taken into account in the individual quoted errors. The measurement errors are summarized in Table 3.

TABLE 3. Measurement errors in branching ratios.

Counting statistics in H	3.6%
Counting statistics in T (depends on target)	3.2 - 7.9%
Errors in π_S^H/π_S^T	10%
Errors in U (depends on target)	5.3 - 8.0%
Overall error in total radiative branching ratios (combine above contributions in quadrature)	10.0 - 14.0%
Fitting errors in partial branching ratios: statistics and correlations (may be large for unresolved lines of a multiplet)	6 - 60%
Acceptance	< 7%

E. Obtaining Rates of Reaction from Branching Ratios

In order to convert branching ratios per stopped pion into rates of reaction (which is the quantity predicted by theory and comparable to other reactions), the total disappearance rate of "lifetime" of stopped π^- in the target material of interest must be known. This rate is deduced from pionic x-ray line widths. If pions are captured from several different atomic orbitals, the total width of each orbital must be known, as must the relative capture fractions. For nuclei with $10 < A < 24$, more than 90% of the capture is from the pionic p orbitals. Theoretical predictions must comprise appropriately weighted sums of capture rates from each of the relevant orbitals. The treatment of these effects has been discussed in detail.[19] Unfortunately the total disappearance rates required are often known only poorly if at all, as are the capture schedules. The pionic atom data used in the present work is summarized in Table A-3 of Appendix A.

V. THEORETICAL BACKGROUND

In this section, notation and formulae from the literature used in the interpretation of the present work are given. These include expressions allowing the extraction of nuclear reduced matrix elements from experimental data on inelastic electron scattering, beta decay, and radiative pion capture. The references, notation and derivations are discussed in Appendix B.

The radiative pion capture rate leading from nuclear state $|J_i\rangle$ to state $|J_f\rangle$ from pionic orbital $\phi_{n\ell_\pi}$ with orbital angular momentum ℓ_π is[40,41]

$$W = \frac{16\pi^2 k}{m_\pi (2J_i+1)(2\ell_\pi+1)} \sum_{J,L} \left| \langle J_f \| \sum_{n=1}^{A} M_a(J,L,\ell_\pi;r_n) \| J_i \rangle \right|^2 + \left| \langle J_f \| \sum_{n=1}^{A} M_b(J,L,\ell_\pi;r_n) \| J_i \rangle \right|^2 \quad . \tag{V-1}$$

The operators M_a and M_b are determined from the elementary process of pion photoproduction on the nucleon, and used to calculate nuclear transition rates in the impulse approximation. In the present work, the terms contributing to transitions from $J^\pi = 0^+ \to 1^+$, $0^+ \to 2^-$, $1/2^- \to 3/2^-$, and $1/2^- \to 5/2^+$ have been worked out explicitly from expressions in Ref. 41 and are shown in Appendix C. These expressions have been used to extract phenomenological matrix elements from the (π^-,γ) data for comparison with other probes and with estimates of single particle strength.

The $ft_{1/2}$ value for pure Gamow-Teller beta decay of a state with spin J_i is related to the reduced matrix element of the spin density operator by

$$ft_{1/2} = 318 \frac{2J+1}{|\langle J_f \| [\sigma \otimes Y_0]^1 t^- \| J_i \rangle|^2} \quad . \tag{V-2}$$

The matrix element $[\sigma x Y_0]^1 t^-$ is proportional to the Gamow-Teller matrix element σt^-. The notation $[\sigma x Y_\ell]^J$ will be used throughout this work for the multipole moments of the (vector) spin density. The mathematical definition is given in Appendix B, as is a discussion of the derivation of the above equation.

The results of inelastic electron scattering experiments are often stated in terms of Γ_0, the radiative width for decay of the upper state J_i into the ground state J_f calculated with the inelastic scattering matrix elements. For an M1 decay, the width may be obtained in terms of the matrix elements from Eq. (21) in Ref. 42:

$$\Gamma_0 = \frac{1}{2J_i+1} \left(\frac{\langle T_f T_f 3 10 | T_i T_i 3 \rangle_\gamma}{\langle T_f T_f 3 1-1 | T_i T_i 3 \rangle_\beta} \right)^2 E_{fi} e^2 \left(\frac{q}{2M}\right)^2 \frac{8\pi}{3} \left| L_{01} + \frac{g_p - g_n}{2} R_{01} \right|^2 . \tag{V-3}$$

Here the notation $L_{\ell J} = \langle J_f \| [L \otimes Y_\ell]^J t^+ \| J_i \rangle$ and $R_{\ell J} = \langle J_f \| [\sigma \otimes Y_\ell]^J t^+ \| J_i \rangle$ has been introduced. The Clebsch-Gordan factor accounts for the rotation in isospin space required by the use of the charge-changing matrix elements $R_{\ell J}$ and $L_{\ell J}$ in this electromagnetic width. The Clebsch-Gordan coefficient in the numerator refers to the isospin quantum numbers of the states involved in the radiative decay, and the denominator refers to the quantum numbers involved in the analog beta transition.

The simple relation between matrix elements containing $t^\pm$ (from charge changing transitions) and those containing t_3 (from electromagnetic transitions) is implied by the isospin symmetry of nuclear wave functions.

This symmetry has been shown to be valid to 10-15% in the widths for M1 transitions in A = 12 [Ref. 42] and A = 13 [Refs. 43 and 44]. In A = 20, the M1 decay of ^{20}Ne (10.27 MeV, $T,T_3 = 1,0$) to the 1.63 MeV, $T,T_3 = 0,0$ state of ^{20}Ne has been compared to the analog beta decay ^{20}F g.s. $\rightarrow$ ^{20}Ne (1.63 MeV) + $e^- + \bar{\nu}_e$, and the results[45] were shown to be in agreement with shell model calculations using identical wave functions for the analog states. The agreement with similar shell model calculations obtained in the present work from the radiative pion capture combined with the 11.24 MeV $T,T_3 = 1,0 \rightarrow$ g.s. M1 decay, may be taken as additional evidence for isospin symmetry in these states.

VI. RESULTS AND DISCUSSION FOR ^{13}C

A. $^{13}C(\pi^-,\gamma)^{13}B$ Spectrum, Branching Ratios and the Pole Model for Quasifree Radiative Capture

The photon spectrum for this reaction is shown as Figure 4a. The fitted curve is shown in Figure 4b. This curve includes four sharp lines, one Breit-Wigner resonance, and the pole model continuum parametrization discussed below. The fitted curve gives a reasonable account of the data (χ^2 = 494 for 487 D.F.) except in the low energy region (E_γ < 85 MeV), where the pole model overestimates the strength.

The partial branching ratios to the various fitted parts of the spectrum are given in Table 4.

The energies of isolated lines are known to within ±100 keV, from comparison with the hydrogen calibration spectrum and the sensitivity of χ^2 to line shifts. The energies given are rounded best fit values. N_{fit} is the number of "counts" assigned by the fitting program to the feature of interest, including the effect of the ratio of the acceptance at the fitted line position to that at E_0 = 129.4 MeV; N_{tot} is the sum of the counts in all the fitted features, which for a perfect fit is equal to the number of events in the experimental histogram, multiplied by the unfolding factor discussed in Section V.C.

The fitting errors discussed in Section V.D contribute little to the uncertainties of the partial branching ratios in this spectrum, except for the small line at 121.5 MeV, where the overall uncertainty becomes 30%.

The smooth continuum photon emission seen above the $(\pi^-,\gamma n)$ threshold in radiative pion capture spectra presumably results from the

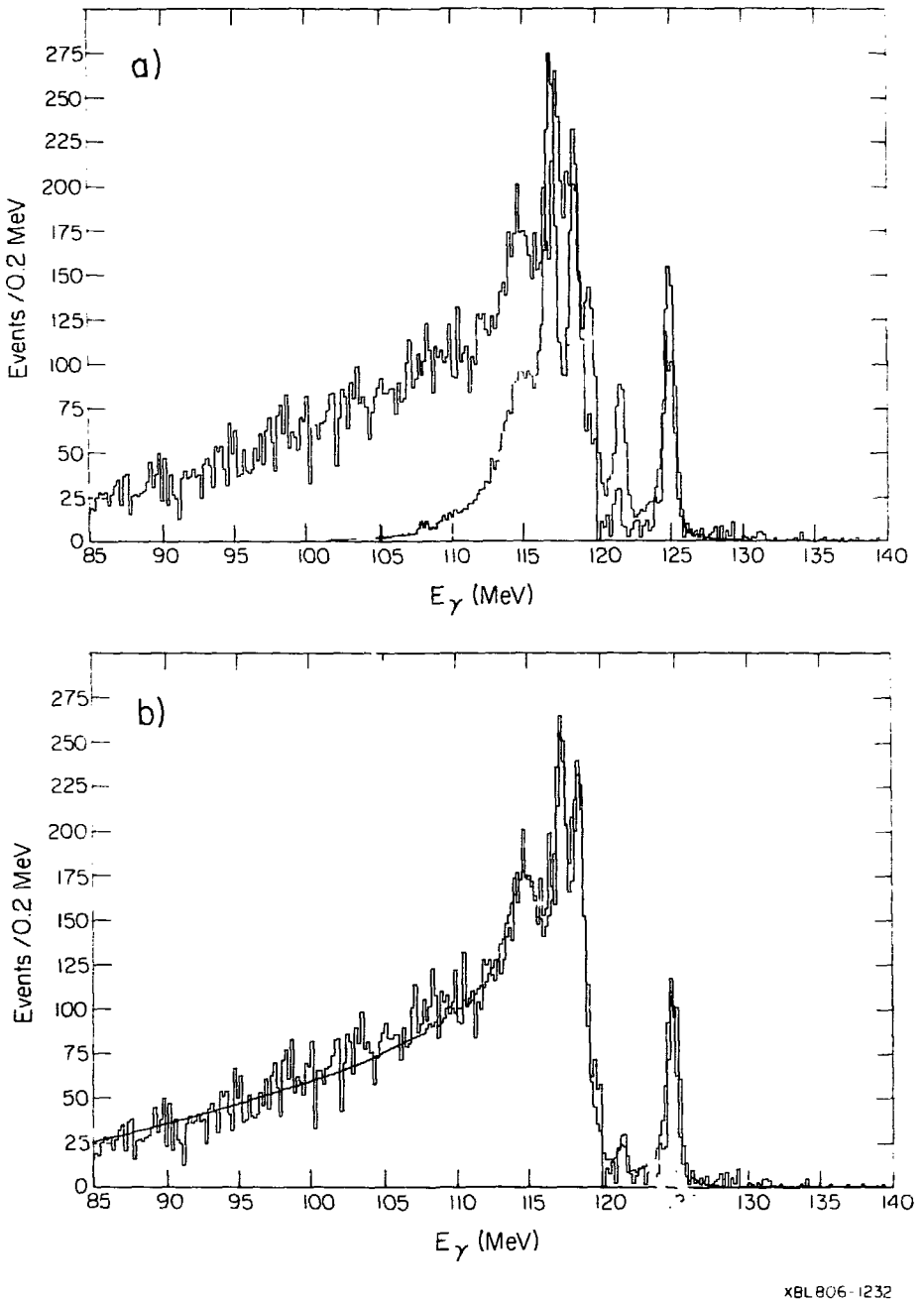

Fig. 4. a) Photon spectrum from radiative pion capture in ^{13}C. b) Experimental spectrum of part a) with fitted curve superimposed. This curve gives the partial branching ratios of Table 4.

radiative capture with a three (or more) body final state, $^{13}C(\pi^-,\gamma+xn)^{(13-x)}B$. This continuum is well fitted by an expression derived from consideration of a one nucleon-pole-model[46] for the quasi-free emission process:

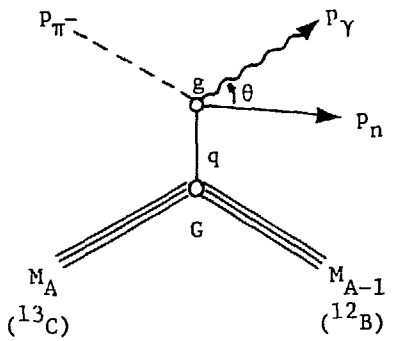

One-nucleon-pole model graph for quasifree radiative capture.

The transition probability is taken as proportional to

$$W_{fi} \sim \frac{Gg\, d^4p_{^{12}B}\, d^4p_n\, d^4p_\gamma}{(q^2-M^2)^2} \times \delta^4(p_{^{12}B^*} + p_n + p_\gamma - p_{\pi^-} - p_{^{13}C}) ,$$

$$q^2 = (p_n + p_\gamma - p_{\pi^-})^2 = \text{4-momentum transfer squared} .$$

There are a number of approximations involved here; final state interactions of the neutron are neglected and a free particle propagator for the exchanged proton is used. When fitting to data, a single mass value for the recoil nucleus is used as a free parameter; in reality one would expect a number of different final states to contribute. The normalization is also fitted to the data. However, the spectrum, derived by carrying out the indicated integrations, provides a convenient universal

fitting function, and the best-fit value of the recoil mass usually comes out within 0.5 MeV of the recoil nuclide ground state mass for light nuclei.

The Continuum Shell Model has been used (with considerable success) to calculate the quasifree component of radiative pion capture spectra more rigorously.[41] In these calculations, the shell-model basis is extended to include states with one nucleon in a continuum state, with distortions by the residual nucleus included. For the cases that have been studied, [$^{12}C(\pi^-,\gamma)$ and $^{16}O(\pi^-,\gamma)$], both the shape and normalization of the quasifree component are given correctly by the calculations.

B. Qualitative Discussion of $^{13}C(\pi^-,\gamma)^{13}B^*$ Spectrum; Comparison with Shell Model Calculations

The photon energies corresponding to transitions leaving the ^{13}B recoil nucleus in particular final states may be calculated from kinematics.[19] By identifying[44] the ^{13}B ground state as the isobaric analog of the 15.106 MeV $T = 3/2$, $J^\pi = 3/2^-$ state in ^{13}C seen in inelastic electron scattering[47] and using a constant energy shift, one can also give an excitation energy scale relative to ^{13}C. This has been included in Tables 4, 5 and 6. By studying level schemes and the e,e' literature, the peaks in the (π^-,γ) spectrum may be identified with states observed by other workers, as shown in Table 5.

Firm quantum number assignments are available from other experiments only for the lowest state. The (π^-,γ) reaction is not selective enough to allow additional quantum number assignments to be made. However, detailed shell model calculations for the (π^-,γ) reaction by

TABLE 4. Partial (π^-,γ) branching ratios for ^{13}C.

E_γ	E_x ^{13}C	E_x ^{13}B	$R_\gamma \cdot 10^{-4}$	R/R_{tot}	N_{fit}
125.0	15.1	g.s.	6.08 ± 1.2	3.66 %	704 ± 50
121.5	18.6	3.5	0.96 ± 0.4	0.58	112 ± 51
117.4	22.7	7.6	8.63 ± 1.7	5.20	998 ± 105
118.5	21.6	6.5	10.23 ± 1.8	6.16	1,183 ± 197
114.8, Γ = 2.14 MeV	25.3	10.2	17.35 ± 3.7	10.45	2,007 ± 286
Pole, Δ = 18.83	--	--	122.74 ± 19.6	73.94	14,200 ± 359
				100.0	19,204

Total radiative branching ratio (166 ± 25) · 10^{-4}

TABLE 5. States excited by (π^-,γ) and by other reactions for ^{13}C.[a]

	Present Work		Other Experiments		
E_γ	E_x ^{13}B	E_x ^{13}C	E_x ^{13}B	E_x ^{13}C	J^π, T
125.0	0.	15.1	g.s.	15.106	$3/2^+$, $3/2$[a]
121.5	3.5	18.6	3.53, 3.68	18.75	$3/2^+$, $5/2^+$, $3/2$[b]
118.5	6.5	21.6	6.419	21.81	$5/2^+$, $3/2$[a]
117.4	7.6	22.7	7.52, 7.86	--	$5/2^+$, $3/2^+$, $3/2$[b]
114.8	10.2	25.3		25.5	$5/2^+$, $3/2^+$, $3/2$[b]

[a] From Tables 13.1 and 13.4 in Ref. 49.

[b] Quantum number assignment from shell model calculation, Ref. 48.

Kissener et al[48] predict groups of $3/2^+$ and $5/2^+$ resonances at 3.8, 6.0, 8.0 and 10.2 MeV excitations relative to ^{13}B. Their predictions for capture rates are in good agreement with the results of the present experiment if the preferred value of $\Gamma_{2p} = 1.95$ eV is used to compute the branching ratios instead of the value 1.02 eV used in Ref. 48. The correspondence is illustrated in Table 6 and in Figure 5, where the theoretical curve is folded with the experimental resolution and plotted on the same scale as the data of Figure 4.

The $5/2^+$ assignment for the 21.6 and 22.7 MeV E_x lines is also supported by the observation by Bergstrom et al[50] of considerable strength in $^{13}C(e,e')$ at backward angles near 22.5 MeV excitation. These authors suggested that this represented magnetic excitation strength.

Kissener and coworkers[48] also predicted an additional state at $E_\gamma = 119.6$ MeV with $R_\gamma = 7 \cdot 10^{-4}$. This state was not observed.

The calculations of Ref. 48 included ground state correlations and a limited number of $2\hbar\omega$ bases states. The older calculations where ground state correlations were neglected[51] typically overestimated pion and muon capture rates as well as e,e' cross sections by a factor of 2. The agreement obtained here shows that such medium energy processes can now be treated quantitatively within the harmonic oscillation shell model.

C. Comparison of $^{13}C(\pi^-,\gamma)^{13}B$ g.s. with $^{13}B \rightarrow {}^{13}C + e^- + \bar{\nu}_e$; Numerical Values of Spin Flip Matrix Elements

The line at 125.0 ± 0.1 MeV corresponds to the pion capture leading to the ground state of ^{13}B. The calculated photon energy for the transition is 124.951 ± 0.004 MeV.

The transition between these states has also been observed in ^{13}B β^-

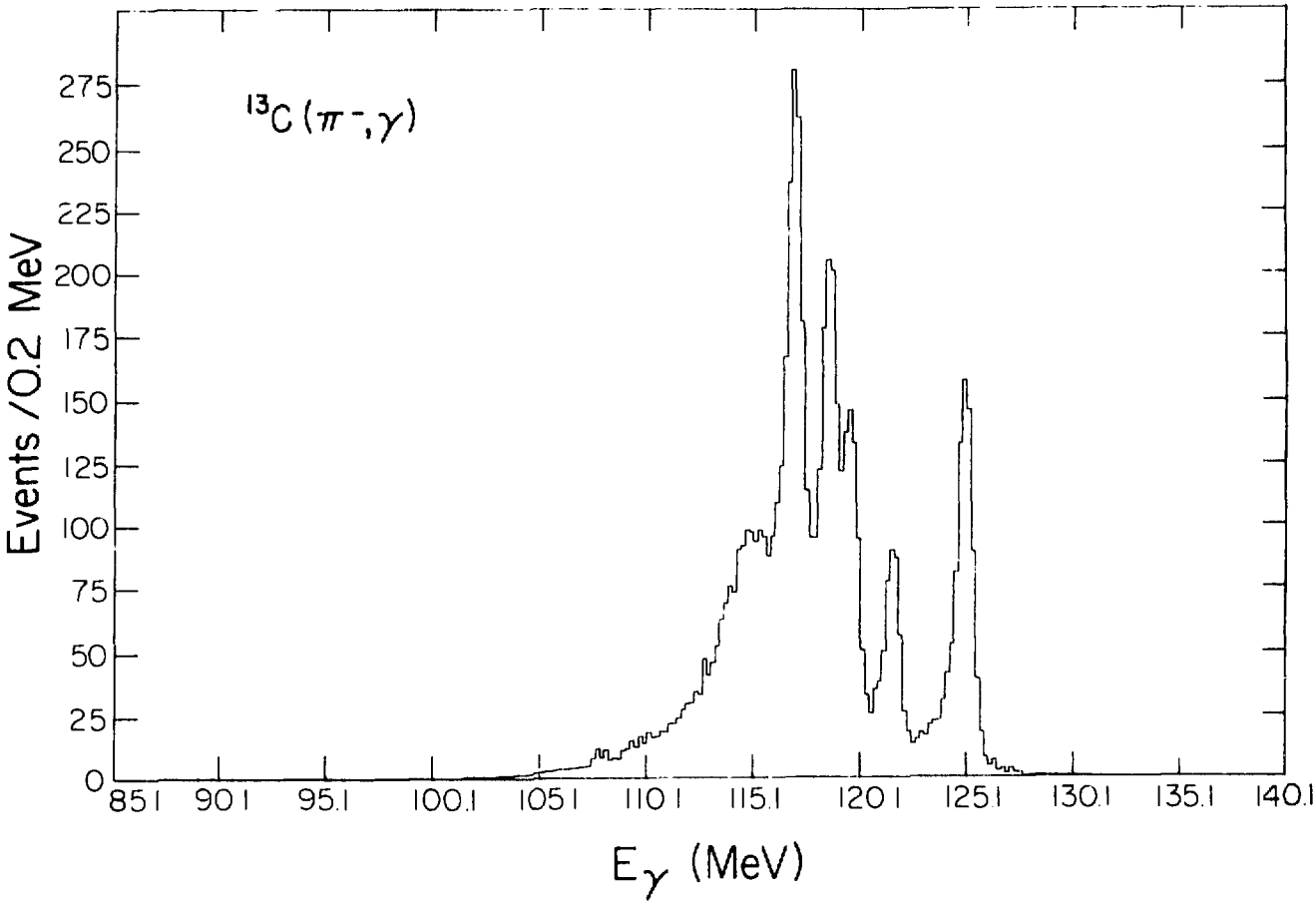

Fig. 5. Predicted photon spectrum for radiative pion capture in ^{13}C from Ref. 52. The curve is properly normalized using the 2p width Γ_{2p} = 1.95 eV, and the data of Fig. 4a are superimposed. XBL 806 1313

TABLE 6. Comparison of calculation of Ref. 52 with experiment. (Predicted excitations lying too close to be resolved in the present experiment have been added together. The theoretical values have been corrected to use $\Gamma_{2p} = 1.95$ eV.)

E_γ	R_γ, Expt ($\times 10^{-4}$)	R_γ, Theory ($\times 10^{-4}$)	J^π, Theory
125.0	6.08 ± 1.2	8.8	$3/2^+$
121.5	0.96 ± 0.4	4.8[a]	$3/2^+$, $5/2^+$
119.6	--	7.0	$3/2^+$
118.5	8.63 ± 1.7	9.4[b]	$5/2^+$
117.4	10.23 ± 1.8	13.1[c]	$5/2^+$, $3/2^+$
114.8	17.35 ± 3.7	14.6[d]	$5/2^+$, $3/2^+$

[a] (States at 121.5 and 121.1 MeV)

[b] (State at 118.6 MeV)

[c] (States at 116.5, 117.0, and 117.2 MeV)

[d] (Sum from 113-115 MeV)

decay,[53] and the ft value measured. Referring to the formulae presented in Section V, one sees that the β decay rate determines the square of the spin density matrix element R_{01}. Calculating by methods discussed in Appendix B, it can be shown that the radiative pion capture branching ratio R_γ to the ^{13}B g.s. is given by an expression of the form

$$R_\gamma = p|R_{01}|^2 + q|R_{22}|^2 + s|R_{21}|^2 + \text{(smaller term.)}$$

where the coefficients p, q, s are determined by the impulse approximation Hamiltonian using harmonic oscillator radial wave functions. Therefore together the two measurements constrain the sum $q|R_{22}|^2 + s|R_{21}|^2$, where R_{22} represents the spin flip E2 part of the transition and R_{21} is an M1 contribution. The inclusion of a third datum from electron scattering is discussed in the next section.

From the $ft_{1/2}$ value for ^{13}B beta decay ($\log_{10} ft_{1/2} = 4.02 \pm 0.02$; Ref. 53) one obtains with Eq. (V-2),

$$R_\gamma = 3.172 \cdot 10^{-3} \left\{ |R_{01}|^2 + 0.705\ |R_{22}|^2 + 0.0697|R_{21}|^2 + 0.0723|Y_2|^2 - 0.0377\ \text{Re}\ R_{22}Y_2 - 0.0251\ \text{Re}\ R_{01}\ R_{21} \right\} \tag{VI-1}$$

For convenience, errors in the coefficients do not appear in the formula, but they are considered in the analysis. These coefficients are obtained with $r_0 = 1.881 \pm 0.053$ fm [Ref. 44] for the harmonic oscillator parameter and including both 1s and 2p capture.

There are a lot of terms in this expression because the transition ($J^\pi = 1/2^- \rightarrow 3/2^-$) can have M1 as well as E2 contributions.

The matrix elements in Eq. (VI-1) are the t^+ (charge lowering) analogs of matrix elements whose t_3 components occur in electromagnetic

transitions.[54] R_{01} is the analog of the spin flip M1 matrix element in the long wavelength limit; R_{21} results from the finite wavelength correction term to the M1 operator; R_{22} is the analog of a spin flip E2 matrix element, and Y_2 is analogous to the long wavelength limit E2 matrix element (charge quadrupole moment).

If the value $|R_{21}| = 0.101 \pm 0.006$ obtained above from beta decay is inserted into this expression and all the other terms are neglected, $R_\gamma = (3.8 \pm 1.2) \cdot 10^{-4}$ is predicted. (The error includes variation of r_0, the beta decay lifetime, and the uncertainties of the π-N coupling constants in the impulse approximation Hamiltonian.) This value is inconsistent with the present measurement $R_\gamma = (6.1 \pm 1.2) \cdot 10^{-4}$, indicating the importance of contributions other than the Gamow-Teller term R_{01}.

D. Remarks on $^{13}C(\pi^-,\gamma)^{13}B$ g.s. and Electromagnetic Data

The preceding section showed that the observed radiative pion capture rate is not accounted for by the Gamow-Teller matrix element known from ^{13}B beta decay. However, the three other matrix elements contributing to the transition (see Eq. VI-1) cannot be separately evaluated from the pion capture data alone.

A value of Y_2 can be taken from the measured E2 decay admixture of the ^{13}C 15.11 MeV state. Using $\Gamma_o(E2) = 0.59 \pm 0.11$ eV from Ref. 55, and formulas 2.32 and 2.33 of Ref. 54, one obtains in the present notation $|Y_2|^2 = 1.14 \pm 0.2$. Inserting this into equation VI-1 along with the value for R_{01} given in the preceding section, one obtains $R_\gamma = (6.4 \pm 1.3) \cdot 10^{-4}$, in agreement with the experimental value

$(6.1 \pm 1.2) \cdot 10^{-4}$ from Table 4. The contributions from R_{21} and R_{22} are thus seen to be small or to cancel each other, to within the experimental errors.

In principle, values of R_{22} and the linear combination $L_{21} + \frac{g_p - g_n}{4} R_{21}$ could be obtained from electroexcitation of the ^{13}C 15.11 MeV level at high momentum transfer, as can be seen from the formulas in Appendix B. Then, inserting the values of Y_2 and R_{22} so obtained into Eq. VI-1, R_{21} could be obtained separately. The high momentum transfer M1 strength proportional to $L_{21} + \frac{g_p - g_n}{4} R_{21}$ could then be separated into its spin flip (R_{21}) and orbital magnetization (L_{21}) parts, just as the low momentum transfer M1 strength can be separated into its spin flip (R_{01}) and orbital magnetization (L_{21}) parts by combining Gamow-Teller beta decay rates with the analogous M1 decay widths.

However, several caveats must be applied to this sort of detailed analysis. The use of values for Y_2 and R_{22} obtained from electromagnetic decays in Eq. VI-1 for the pion capture rate assumes isospin invariance for these E2 admixtures. Although the experimental evidence favors isospin invariance for M1 widths in A = 13, the E2 admixtures appear to be different for, e.g., the radiative decays of ^{13}N (15.07 MeV) and ^{13}C (15.11 MeV).[43]

The free interchange of matrix elements measured with different probes also ignores possible effects due to meson exchange currents. These have been calculated to contribute 30% to the electromagnetic widths at the momentum transfers under consideration.[56] The meson

exchange contributions to pion capture are expected to be different,[57] and their influence on the reaction considered here has not been computed.

Finally, electroexcitation data in the region of momentum transfer needed to determine R_{21} and R_{22} ($250 \lesssim q \lesssim 350$ MeV/c) have not been published.

To summarize the results of this section: the measured branching ratio for $^{13}C(\pi^-,\gamma)^{13}B$ g.s. is correctly given by the Gamow-Teller matrix element known from ^{13}B beta decay and an E2 contribution calculated from the charge quadrupole moment matrix element Y_2 measured by the E2 admixture in ^{13}C (15.11 MeV) radiative decay to the ^{13}C ground state. More experimental data of better precision, as well as more sophisticated theoretical treatment will be needed to study the high momentum transfer spin flip matrix elements R_{21} and R_{22}.

E. Giant Resonance Excitation in $^{13}C(\pi^-,\gamma)$

As mentioned in Chapter II, the idea of giant resonance excitation has been important in the historical development of nuclear π and μ capture.

The E1 photoresonance results from the action of the electric dipole operator ($e\vec{r} \sim t_3 Y_1$ in the present notation) on the nuclear ground state. The very large strength associated with the resonance can be understood if one notes that a collective oscillation of protons against the C.M. will be set up by a harmonic perturbation of the form $t_3 Y_1$. This amounts to an oscillation of protons against neutrons if the C.M. stays fixed.[58] The motion can be envisioned as an eigenmode of a two-fluid system, with a restoring force given by the symmetry energy term in the semiempirical mass formula. This "schematic model" originated by Gamow and Teller[59] accounts surprisingly well for the energy and strength of the E1 photoresonance.

To understand the photoresonance in the context of the shell model, one notes that the operator $t_3 Y_1$ would appear to excite a single particle into the next L shell. Such single-particle states are observed, but they have extremely small strengths, and their excitation energies are $\lesssim$10 MeV. The photoresonance lies much higher, e.g. 23 MeV in ^{12}C. This contradiction was resolved by Brown and Bosterli,[32] who recognized the near-degeneracy of many single-particle excitations available to the valence nucleons. This degeneracy leads to strong mixing of the states by small residual interactions not included in the zero-order shell model Hamiltonian. Their model calculation showed concentration of all the transition strength into a single level, and

a considerable upward shift in energy for that level.

In the case of radiative pion capture, the operators $t^+R_{\ell J} = t^+[\sigma x Y_1]_{0,1,2}$ occur. In analogy to t_3Y_1, one can envision hydrodynamical modes excited by these operators in which neutrons with spin up and protons with spin down ($\sigma t > 0$) oscillate against neutrons with spin down and protons with spin up[14] ($\sigma t < 0$). The restoring force in this case would be more complicated, involving spin-exchange forces[12] and possibly the surface energy.

Dogotar et al have discussed these ideas in the shell model picture.[52] The $\Delta J = 2$ resonances are expected to be strongest because of the statistical factor $2J + 1$ in the number of final states. By arguments involving the configuration of the ground state and the $\Delta L = 1$ selection rule for the operator $t^+R_{\ell J}$, they qualitatively explain the presence and absence of sharp peaks at high excitation in (π^-,γ) on most of the 1-p shell odd-A nuclei. Because of its ground state configuration, ^{13}C is expected to show very prominent $J^\pi = 5/2^+$ peaks. Comparison of the experimental data with the results of their detailed calculations as presented in Section VI.B and Table 6 seems to bear out these ideas.

However, the degree of collectivity of these states is not clear from the published calculations. Since for many people the identification of an observed excitation as a giant resonance hinges on the degree of collectivity, it was thought worthwhile to investigate this question. Therefore, the theoretical expressions of Ohtsubo et al[40] used in the preceding section on M1 transitions have been extended to the case of $\Delta J^\pi = 2^-$ transitions. Ohtsuka[41] also gives formulae for

the values of Y_J and $R_{\ell J}$ that would result from a single particle transition between pure configurations of given L and J. These are computed from vector coupling algebra only. The matrix element values derived from the observed branching ratios may be compared with these "single particle" values.

It is interesting to first compare the M1 matrix elements with the single particle values. One obtains $R_{01}^{SP} = 0.65$ assuming a pure $p_{3/2} \rightarrow p_{1/2}$ transition. The observed value $R_{01} = 0.348$ represents 0.53 single particle units. This is typical for the so-called giant M1 transitions in the 1p shell.[60] In fact, it can be shown that an M1 transition strength of this magnitude nearly exhausts the energy weighted sum rule on the total M1 strength developed by Kurath.[61] The small sum rule value may be understood in terms of the limited number of unsaturated spins able to undergo pure-spin-flip M1 transitions.

For the case of R_{12} one obtains a single-particle estimate of $R_{12}^{SP} = 0.62$. Inserting this value into Eq. (V-1) for the radiative capture rate with the appropriate coefficients from Appendix 3 (neglecting all terms not containing R_{12}), one obtains a single particle branching ratio estimate of $2 \cdot 10^{-3}$. The observed values for the high lying states (Table 4, p. 33) range from 0.9 to $1.7 \cdot 10^{-3}$ per state, corresponding to unsquared matrix elements of 0.7-0.9 single particle units per state. The total branching ratio to the three fitted peaks is $3.6 \cdot 10^{-3}$, equivalent to 1.4 single particle units in the amplitude. This estimate specifically excludes pole-model strength lying at energies equal to and less than the fitted peaks. A degree of collectivity is definitely indicated for these resonances. One should note

that the four $1p_{3/2}$ protons are essentially the only active nucleons for these transitions. (Transitions involving promotion of 1s nucleons through one ℓ shell are blocked by the nearly full 1p neutron shell. Such transitions are observed in cases where the 1p shell is nearly empty (e.g., ^{6,7}Li or ^{9}Be; see discussion in Refs. 48 and 52). They occur at much higher excitation energy (15-25 MeV in the recoil nucleus) than the peaks presently being considered (7-10 MeV in the recoil nucleus).

Although generally accepted forms for M1 (Ref. 61) and E1 (Ref. 31) sum rules exist in the literature, a satisfactory M2 form cannot be derived in a compelling fashion.[31] This is due essentially to the relatively complicated coupling of spin and spatial degrees of freedom in R_{12}. Therefore a discussion of these M2 resonance strengths in terms of an M2 sum rule is not presented.

Some remarks should be made as to the strength of the E1 photoresonance, however. In ^{13}C the (γ,n) cross section integrated from 5 to 42 MeV excitation exhausts 65% of the Thomas-Reiche-Kuhn sum rule.[62] Roughly 60% of this strength may be attributed to T = 3/2 excitations (21.7 MeV to 42 MeV).[62] Therefore, if the full sum rule value is taken to represent Z = 6 single particle units, the T = 3/2 photoresonance represents only 3.8 single particle units in the amplitude. This is to be compared to the estimate of 1.4 units obtained above for the M2 giant resonance excitations in (π^-,γ).

Alternatively, one may use the formula

$$\sigma = \frac{\alpha}{2\pi} \left| \langle J_f \| Y_1 \| J_i \rangle \right|^2 \langle r^2 \rangle$$

for E1 photoabsorption[63] with the total cross section value of σ = 6.5 mb given in Ref. 62 for photoabsorption between 19-30 MeV, to estimate $|\langle J_f \| Y_1 \| J_i \rangle|$ = 2.7. The "single particle" value obtained as before from formulae in Appendix B of Ref. 41 is 0.76. The T = 3/2 states in this energy region comprise about 75% of the observed strength, so one again obtains an estimate of three single particle units for the T = 3/2 photoneutron data.

These considerations indicate that the group of strong excitation observed in the $^{13}C(\pi^-,\gamma)$ spectrum do have a strength nearly half that of the E1 photoresonance, in appropriate units.

Another criterion for giant resonance of nuclear matter is that the excitation should be seen throughout the periodic table.[64] This is not the case for the excitations considered here. Nuclei above $A \gtrsim 20$ show only some weak (compared to the smooth quasifree contribution) and diffuse structures in the (π^-,γ) spectra. The excitation energies relative to the target are well below the E1 photoresonance peaks[19] (e.g., photoresonance peaks at 18-22 MeV in ^{28}Si; structure in ^{28}Si (π^-,γ) spectrum from 13-15 MeV excitation). In ^{90}Zr (present work) the (π^-,γ) spectrum is practically smooth. This systematic behavior is not well understood. Mottelson has suggested[31] that the M2 single particle response function may be much more spread out than the E1 response, because of the additional gain or loss of spin orbit energy occurring in $\Delta L = 1$, $\Delta S = 1$ transitions. Since the M2 single particle transitions are not nearly degenerate as they were for the E1 case, the weak residual interaction may not have such a profound effect on redistributing the strength. In the light nuclei the low L values mean

that $\Delta L = 1$, $\Delta S = 1$ transitions still lie close together, and the strength can become concentrated and shifted up in energy. The diffuse strength observed in heavy nuclei does occur in the region of unshifted single particle transitions.

However, a correspondence between what concentrated M2 strength is observed in inelastic electron scattering and the structure in the $^{28}Si(\pi^-,\gamma)$ spectrum has been discussed by Perroud.[29] Strong M2 lines are seen in (e,e') spectra at just the energies of the structures in the (π^-,γ) spectra. A similar correlation may be seen for the weaker structure in the $^{24}Mg(\pi^-,\gamma)$ spectrum[19] and the (e,e') data of Fagg and coworkers.[30] It would therefore appear worthwhile to use the extensive compilations of (π^-,γ) data on 1-p shell[19] and s-d shell[65] nuclei as a guide in electron scattering searches for concentrated M2 strength.

VII. RESULTS AND DISCUSSION FOR ^{20}Ne

A. $^{20}Ne(\pi^-,\gamma)^{20}F$ Spectrum and Branching Ratios

The photon spectrum for this reaction is shown in Figure 6a. The fitted curve from which values in Table 7 were determined is shown in Figure 6b. The fit includes four lines, two Breit-Wigner resonance lineshapes and the pole model background parametrization. The pole model parameter has been fixed at the value corresponding to neutron emission leaving ^{19}F in its ground state: $^{20}Ne(\pi^-,\gamma n)^{19}F$ g.s. The fit in this case is not as good as for ^{13}C ($\chi^2 = 613$, 486 DF). The spectrum appears rather broad, and the statistical fluctuations appear unusually large between 122-129 MeV. Some structure is seen that may represent additional excitations. However, these structures were not fitted separately due to the complexity and limited statistics.

TABLE 7. Partial (π^-,γ) branching ratios for ^{20}Ne.

E_γ	E_x ^{20}Ne	E_x ^{20}F	$R_\gamma \cdot 10^{-4}$	$R_\gamma/R_\gamma^{tot} \cdot 10^{-2}$	N_{fit}
131.3	10.2	0.0	0.7 ± 0.3	0.42	71 ± 13
130.2	11.3	1.1	0.9 ± 0.5	0.57	97 ± 58
130.0	11.5	1.3	1.7 ± 0.6	1.07	182 ± 70
129.5	12.0	1.8	2.6 ± 0.4	1.61	274 ± 32
125.2, $\Gamma = 1.35$	16.3	6.1	15.3 ± 1.9	9.55	1630 ± 79
114.2, $\Gamma = 2.7$	27.3	17.1	4.8 ± 1.7	3.0	511 ± 101
pole, $\Delta = 14.4$ MeV	--	--	134 ± 22	83.0	14300 ± 371
		Total	160 ± 24	100.0	17,065

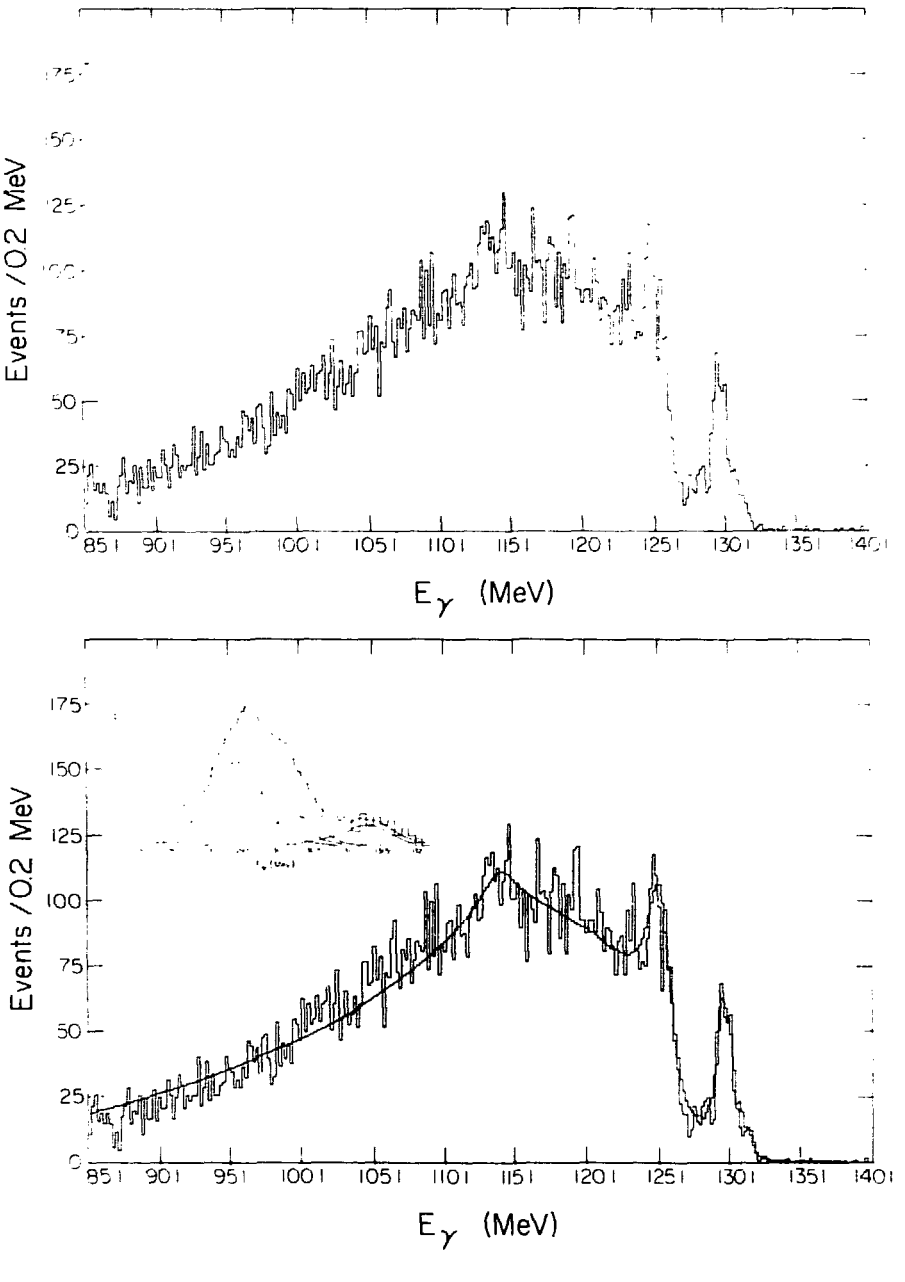

Fig. 6. a) Photon spectrum from radiative pion capture in ^{20}Ne. b) Experimental spectrum of part a) with fitted curve superimposed. This curve gives the partial branching ratios of Table 7. Inset; upper most portion of spectrum on expanded scale (0.1 MeV/bin) with individual fitted peaks shown.

The region around $E_\gamma = 130$ MeV is shown on an expanded scale in the inset of Figure 6a. The spacing of the lines in the fit has been fixed corresponding to the known $J^\pi = 1^+$ and 2^- states of ^{20}F in this region (see next section). The fit has been attempted with the ensemble of lines shifted higher and lower in energy. A 150 keV shift either higher or lower in energy increases χ^2 from 47 to 53 for 31 degrees of freedom. In the calculation of the expected photon energies for the known nuclear masses, the inclusion of the weighted average of the 1s and 2p pionic Ne binding energies was required to obtain agreement with the observed peak positions. This amounts to a 150 keV shift.

The total branching ratio is $(1.6 \pm 0.2)\%$, where the uncertainty reflects that of the normalization data.

B. Qualitative Discussion of $^{20}Ne\ (\pi^-,\gamma)^{20}F$ Spectrum

The photon energy calculated for the $^{20}Ne(\pi^-,\gamma)^{20}F$ g.s. transition is 131.3 MeV. The ^{20}F ground state is the analog of the first T = 1 state in ^{20}Ne, which lies at 10.27 MeV excitation.[66] Assuming a constant energy difference of the analog states in the two nuclides, one may obtain energy scales relative to ^{20}Ne and ^{20}F. The peaks observed in the present work are correlated in Table 8 with states known from other reactions.[66]

Quantum number assignments are available only for the states at low excitation. From previous experience with (π^-,γ) one would expect the higher-lying broad states to have negative parity and spin ≤ 2.

Shell model calculations of $^{20}Ne(\pi^-,\gamma)$ have been reported by Knupfer *et al*[67] but not yet published in any detail. The reported value

TABLE 8. States excited by (π^-,γ) and by other reactions for ^{20}Ne.

	Present Work		Other Experiments		
E_γ, MeV	E_x ^{20}F	E_x ^{20}Ne	E_x ^{20}F	E_x ^{20}Ne	J^π
131.3	0.0	10.2	0.0	10.27	2^+
130.2	1.1	11.3	1.06	11.24	1^+
130.0	1.3	11.5	1.30	11.60	2^-
129.5	1.8	12.0	1.84	12.1	2^-
125.2	6.1	16.3	(four states $6.2 < E_x < 5.9$ MeV in ^{20}F)		
114.2	17.1	27.3	--	--	--

of $R_\gamma = 19 \cdot 10^{-4}$ for the 1^+ state is a factor of 20 higher than our measurements. It exceeds the sum of the branching ratios to the four lowest states by more than a factor of 4. The pionic atom data used to obtain the calculated value were not reported. However, concentration of the whole M2 strength in ^{20}F at 7 MeV was also predicted. It is tempting to identify this with the peak observed at 6.3 MeV. The predicted branching ratio is $40 \cdot 10^{-4}$, higher than the observed value by a factor of 4.

Evidence for isovector spin-flip strength in A = 20 has also been obtained from the (n,p) reaction.[68] The (n,p) data at 60 MeV neutron energy showed excitations at 1.06, 4.2 and 8.0 MeV, with angular distributions favoring orbital angular momentum transfers ≥ 2 for the upper two states. The usual parametrization of the (n,p) quasifree background in terms of the three-body phase space did not fit the ^{20}Ne data as well as it fits data for other targets.[69] This is also the case in the

present work using the pole model parametrization for the $^{20}Ne(\pi^-,\gamma n)^{19}F$ process. χ^2/DF is nearly 30% higher for the ^{20}Ne fit than for ^{13}C. Perhaps alpha-particle breakup (threshold at only 13.3 MeV in ^{20}Ne, 20.2 MeV in ^{13}C) and other complicated final states are involved.

The broad bump around 27 MeV E_x in our photon spectra does not appear to correspond to any feature known from other reactions. The high excitation energy (e,e') spectra of Szalata *et al*[70] extend only to 22.5 MeV excitation for the transverse form factor. Their experiments were performed at forward angles, which would suppress the transverse (spin flip) strength represented by the (π,γ) feature.

C. Comparison of $^{20}Ne(\pi^-,\gamma)^{20}F$, 1.06 MeV with $^{20}Ne(e,e')^{20}Ne$, 11.24 MeV; Numerical Upper Limit on Spin Flip Matrix Element and Lower Limit on Orbital Recoupling Matrix Element

The line at 130.4 MeV appears at the energy expected for the transition to the 1.06 MeV 1^+ state of ^{20}F. This state is the analog of the strong M1 transition observed by Bendel et al[71] in 180° inelastic electron scattering. A calculation of the sort performed above for $^{13}C(\pi^-,\gamma)$ allows one to find limits on the values of R_{01} and L_{01}. Unlike the case of ^{13}C (Ref. 44), the contribution of L_{01} is shown to be nonnegligible. (If the 1.06 MeV level were observed to undergo beta decay, the ft value could be combined with the e,e' data to give values for R_{01} and L_{01}. However, the 1.06 MeV state decays to ^{20}F g.s. with a lifetime of 0.03 ps, so the beta decay is unobservable.)

Using Eq. (V-1) and the formulae of Appendix B, one obtains, with the measured pion capture branching ratio inserted:

$$1 = \frac{|R_{01}|^2}{(0.114)^2} + \frac{|R_{21}|^2}{(0.436)^2} \quad \frac{\mathrm{Re}(R_{01}R_{21}^*)}{(0.98)^2} \quad .$$

The constraint is an ellipse in $R_{01}R_{21}$ space. Matrix elements of R_{L2} operators do not appear because the transition is $0^+ \rightarrow 1^+$. The ellipse represented by this equation is plotted in Figure 7. The maximum value of $|R_{01}|$ permitted is 0.114, with an uncertainty of about ±20% if only the uncertainties in A, B, C, r_0 and R_γ are considered, or ±30% if the uncertainties in the pionic atom data are included.

The electron scattering experimenters[71] reported $\Gamma_0 = 11.2^{+2.1}_{-1.8}$ eV for the radiation width of the 11.24 MeV state in ^{20}Ne. Inserting this value into Eq. (V-3) one obtains

$$\pm(1.16 \pm 0.17) = L_{01} + 4.71\ R_{01} \quad .$$

Taking the + sign and inserting the value $R_{01} \leq 0.114$ from the pion capture data gives $L_{01} \leq 0.62 \pm 0.33$, where the error includes the 30% uncertainty in R_{01}.

Maripuu and Wildenthal[72] and Wildenthal and Chung[24] have performed detailed shell model calculations of the giant M1 transition in ^{20}Ne. Their results have also shown appreciable strength from L_{01}. From results given in Ref. 24, one obtains the present notation $R_{01} = 0.105$ and $L_{01} = 0.605$ (no "errors" for these theoretical values were given), in good agreement with the limits obtained from (π^-,γ) and (e,e').

One can understand the importance of orbital recoupling in this case on the basis of shell model considerations. There are four valence nucleons in ^{20}Ne. These occupy mainly the $d_{5/2}$ orbitals, of which there are twelve. It is therefore possible to obtain a large statistical weight

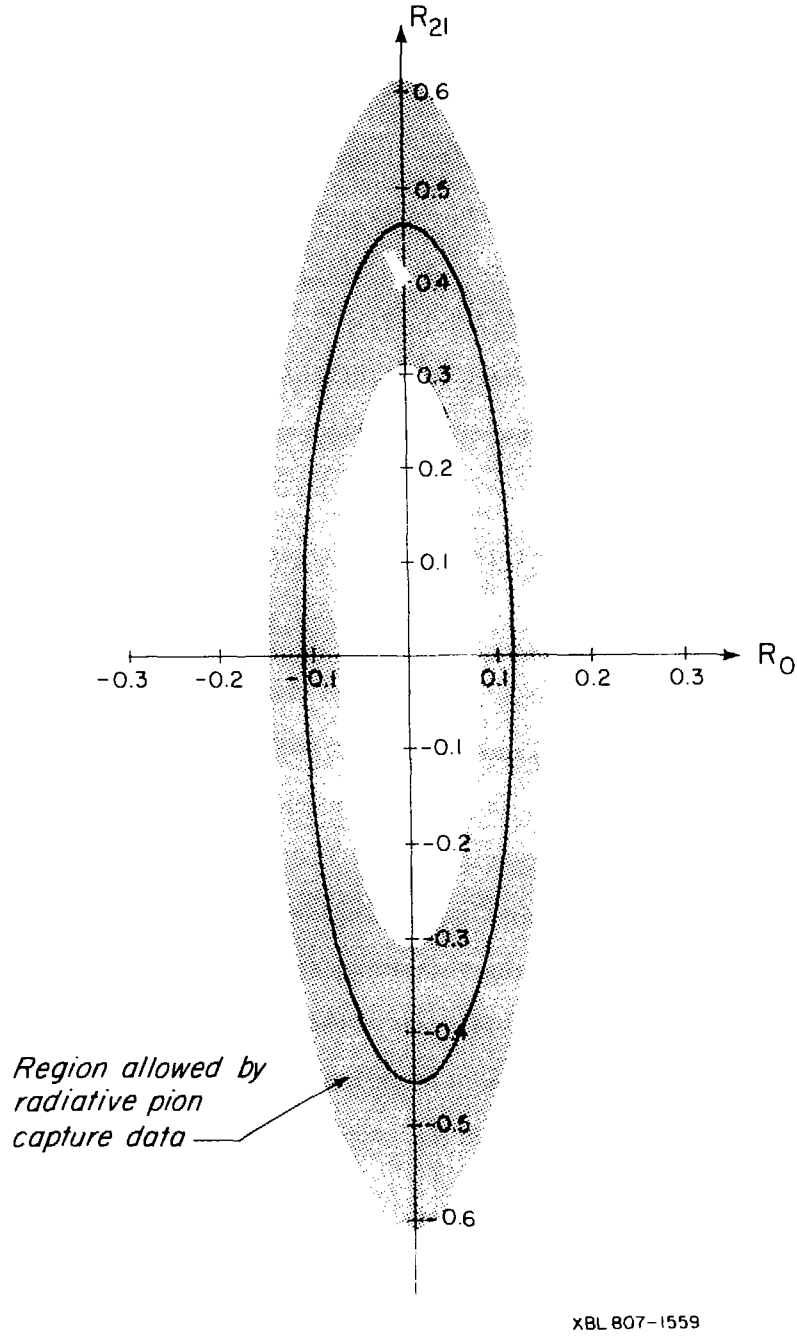

Fig. 7. Constraint on spin-density matrix elements R_{21} and R_{01} obtained from the present work. The shaded region is allowed by the experimental uncertainties. The observed electromagnetic width would require $R_{01} = 0.25 \pm 0.03$ if it were to be all spin flip.

for recoupling the orbital angular momenta within the $d_{5/2}$ orbital to obtain J = 1.

The orbital recoupling terms are also favored over spin flip terms by the following argument. A $d_{5/2}$ state can be written $|5/2,5/2\rangle = |2,2\rangle|1/2,1/2\rangle$. The orbital angular momentum lowering operator acting on this state gives $L_-|2,2\rangle|1/2,1/2\rangle \sim |2,1\rangle|1/2,1/2\rangle$, which contains predominantly J = 5/2, since $|2,1\rangle|1/2,1/2\rangle = \sqrt{4/5}\ |5/2,3/2\rangle - \sqrt{1/5}\ |3/2,1/2\rangle$. On the other hand, the spin-lowering operator acting on $d_{5/2}$ produces mostly J = 3/2:

$$S_-\ |2,2\rangle|1/2,1/2\rangle \sim |2,2\rangle|1/2,-1/2\rangle$$

$$= \sqrt{1/5}\ |5/2,3/2\rangle - \sqrt{4/5}\ |3/2,3/2\rangle \quad .$$

Since it is empirically known that concentrated M1 strength lies in the lower transitions,[61] the orbital recoupling transitions within the $d_{5/2}$ orbital should tend to be enhanced over the spin flip transitions involving the higher-lying $d_{3/2}$ orbital.

In summary, the $^{20}Ne(\pi^-,\gamma)$reaction has been used in combination with inelastic electron scattering data to separate the M1 transition density into its spin-flip and orbital angular momentum-flip parts. The giant M1 transition in this system has been shown to proceed largely through the orbital term, in agreement with theory.

VIII. RESULTS AND DISCUSSION FOR $^{90}Zr(\pi^-,\gamma)$ AND $^{19}F(\pi^-,\gamma)$

The spectra for these targets are shown in Figures 8 and 9.

The ^{90}Zr spectrum is quite featureless. A pole model curve with Δ = 14.1 MeV, corresponding to $^{90}Zr(\pi^-,\gamma n)^{89}Y$ g.s., provides a reasonable fit to the ^{90}Zr data at low photon energies. Excess strength above the fit is noted in the region 12-26 MeV excitation in ^{90}Zr. The total branching ratio is 1.7 ± 0.5%. This corresponds to a radiative pion capture rate of $1.3 \cdot 10^{16}$ sec^{-1}, assuming the capture occurs 100% from the 3d atomic orbital, as shown in Table A3.

The ^{90}Zr target was proposed in hopes of observing the elusive $T_>$ component of the E1 photoresonance by (π^-,γ). This particular resonance has been detected as sharp lines in (p,γ) work.[73,74] The lines expected from the (p,γ) work would appear in (π^-,γ) at E_γ = 116.4 and 117.9 MeV. Excitation of the E1 states via their spin-flip components in the (π^-,γ) reaction does not stand out above the many other states available in this energy region. The capture from $1 \geqslant 2$ atomic orbitals in heavy nuclei allows transitions of many multipolarities, making (π^-,γ) less selective in these cases.

The ^{19}F spectrum (Figure 10) was obtained from ^{Nat}LiF and CF_2 spectra acquired in the present experiment. Spectra for ^{Nat}Li and ^{12}C were provided by P. Truol of the University of Zurich. To avoid making assumptions about the relative capture fractions on the various nuclides, an analytic formula was developed by which the χ^2-minimizing solution to the problem of separating out the ^{19}F spectrum could be obtained. The

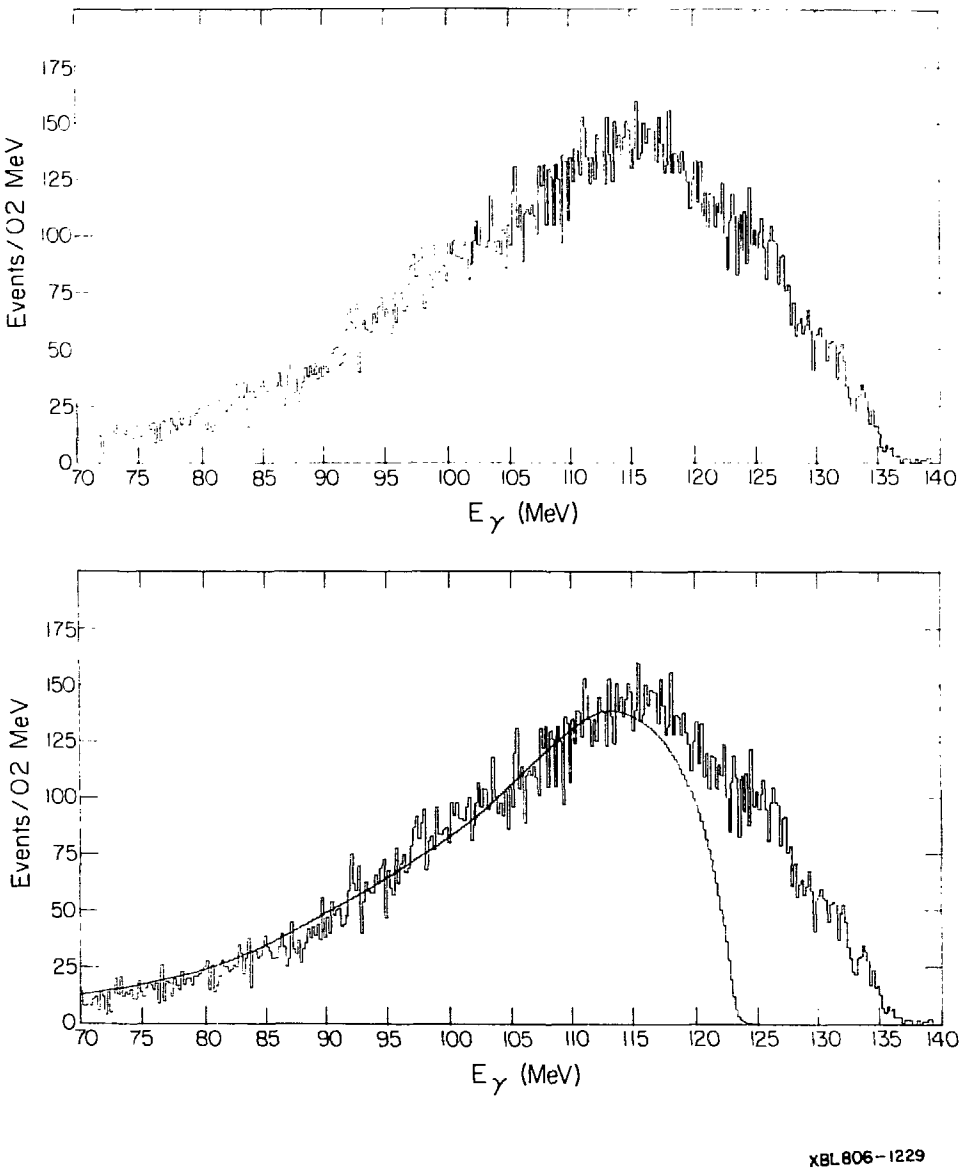

Fig. 8. a) Photon spectrum from radiative pion capture on ^{90}Zr. b) Experimental spectrum of part a) with fitted pole model curve superimposed. This curve is fitted in the low energy region using the expressions of Ref. 46 for $^{90}Zr(\pi^-,\gamma n)^{89}Y$ g.s. Excess strength observed above the γn threshold at 124. MeV is due to $^{90}Zr(\pi^-,\gamma)^{90}Y$.

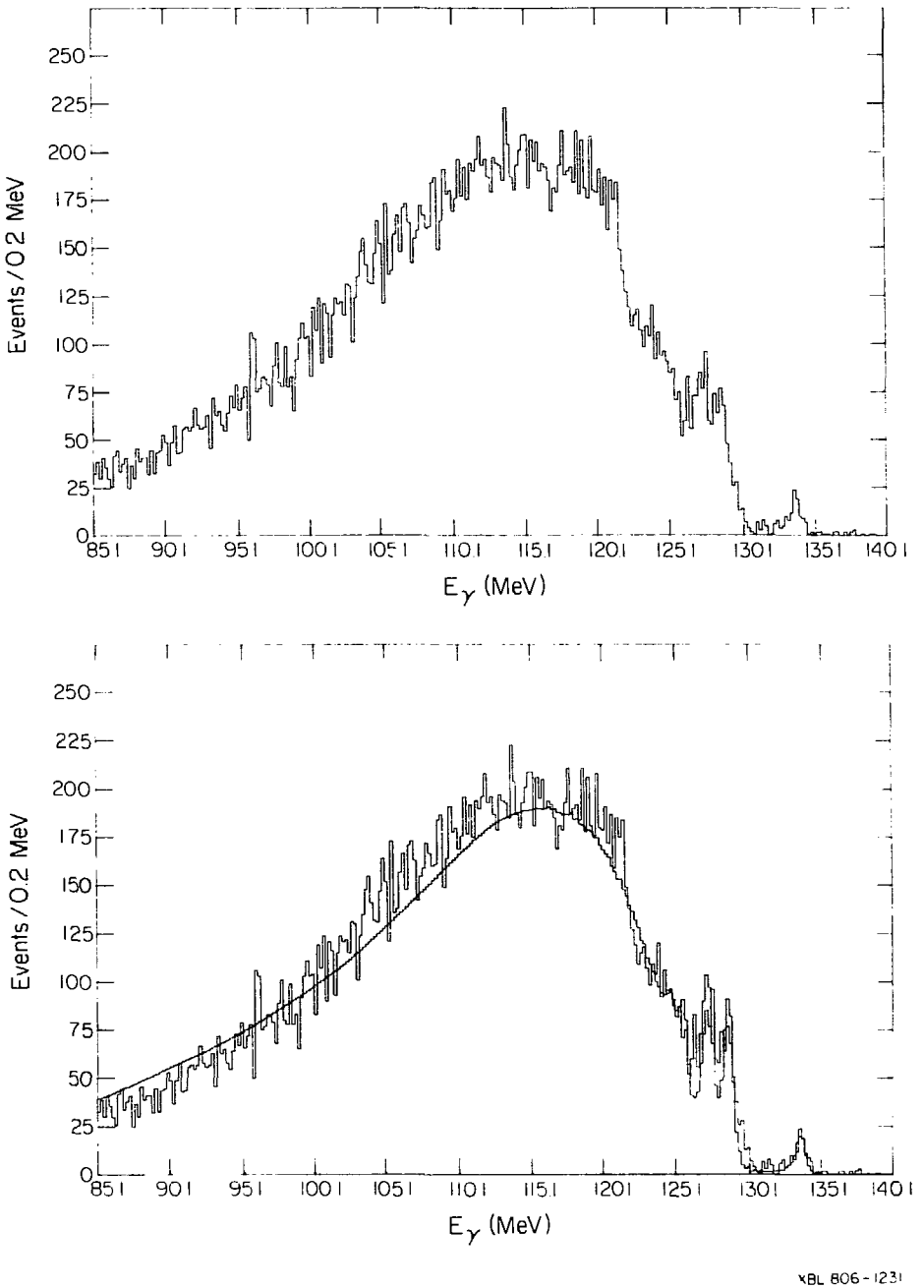

Fig. 9. a) Photon spectrum from radiative pion capture on ^{19}F derived from CF_2 and LiF spectra. b) Experimental spectrum of part a) with fitted curve superimposed. This curve gives the partial branching ratios of Table 9.

formalism is shown in Appendix E. The capture was >80% from ^{19}F in both cases. The total branching ratio for $^{19}F(\pi^-,\gamma)$ is $(2.40 \pm 0.38) \cdot 10^{-2}$.

The interest in $^{19}F(\pi^-,\gamma)^{19}O$ is primarily in observing the systematics, as nucleons are added to the doubly closed nucleus ^{16}O. The spectra of $^{16}O(\pi^-,\gamma)$ and $^{18}O(\pi^-,\gamma)$ are practically identical.[75] Strong core excitations leading mainly to 2^- states ($^{16,18}N$ g.s. and states near 8 and 11 MeV) are seen. In ^{19}F the corresponding core excitations are split by coupling to the valence proton. Lines at energies of known states corresponding to these core excitations in ^{19}O have been included in the fits. However, substantial ambiguity in the fitted strengths arises due to the uncertain pole model fit. It is interesting to note that the best fit value of the pole model parameter corresponds to $^{19}F(\pi^-,\gamma n)^{18}O$ (6.5 MeV). This relatively high excitation is close to the energy of the first negative parity (core excitation) state in ^{18}O at 4.5 MeV, reflecting the dominance of such excitations in this reaction.

Radiative capture to the positive parity states of ^{19}O (valence nucleon excitation) including the $5/2^+$ g.s., the $1/2^+$ and $7/2^+$ at 1.47 and 2.78 MeV respectively with branching ratios less than $0.5 \cdot 10^{-4}$, cannot be excluded. The energies, partial branching ratios, and quantum numbers of discrete states excited in ^{19}O are indicated in Table 9.

TABLE 9. Excitations observed in $^{19}F(\pi^-,\gamma)^{19}O$.

E_γ	E_x ^{19}F	E_x ^{19}O	$R_\gamma \cdot 10^{-4}$	J^π [a]	N_{fit}
133.6	(7.6)	0.0	1.3 ± 0.3	$5/2^+$	166 ± 2
128.6	(11.5)	3.9	4.5 ± 0.9	$3/2^-$ [b]	562 ± 9
127.2	(12.2)	4.6	4.8 ± 1.0	$3/2^-$ [b]	584 ± 18
125.6	(13.9)	6.3	3.2 ± 0.75	$7/2^-$	401 ± 50
124.8, Γ = 0.34 MeV	(18.6)	11.0	3.2 ± 0.7	$(5/2^-)$ [b]	333 ± 23
pole, Δ = 17.8	--	(6.5)	223 ± 46		
	Total		240 ± 48		29,350 ± 381

[a] J^π from Ref. 66.

[b] Corresponds to 2^- excitations noted in $^{16,18}O(\pi^-,\gamma)$.

Blank

IX. RESULTS AND DISCUSSION FOR THE IN-FLIGHT CAPTURE REACTION $^{12}C(\pi^+ 44\ MeV, \gamma)^{12}B$

For nuclear structure studies, the in-flight pion capture has evident advantages over the capture at rest. Momentum/transfer and angular-dependence could be used to obtain transition multipolarities directly instead of relying on other reactions or on theory. The imprecise pionic atom data could be dispensed with and replaced by DWBA or similar calculations constrained to fit elastic scattering. Alternatively, relatively well understood transitions like the giant M1 could be used to give information on the π wave function distortion. Finally, interesting and exotic phenomena such as meson-exchange effects and pion condensation may manifest themselves at momentum transfers $q \sim 2\text{-}3\ M_\pi$ or 280-420 MeV/c.[25]

For these reasons, a feasibility study of $^{12}C(\pi^+,\gamma)$ was undertaken in the present work. The results indicate that the rates are not prohibitively low (1200 radiative events were obtained in 77 hours of beam on target). The cross section is in reasonable agreement with theoretical calculations based on electron scattering matrix elements.

The target was graphite, 1.35 g/cm^2 or 4.0 MeV thick to 46 MeV pions. The pion beam energy at the center of the target was 44.0 MeV. The photon spectrum is shown in Figure 10. From the photon energy and the angle of emission relative to the incident beam the invariant mass of the recoiling system can be deduced. The invariant mass spectrum is plotted as Figure 11, where the mass of the ^{12}N ground state has been subtracted.

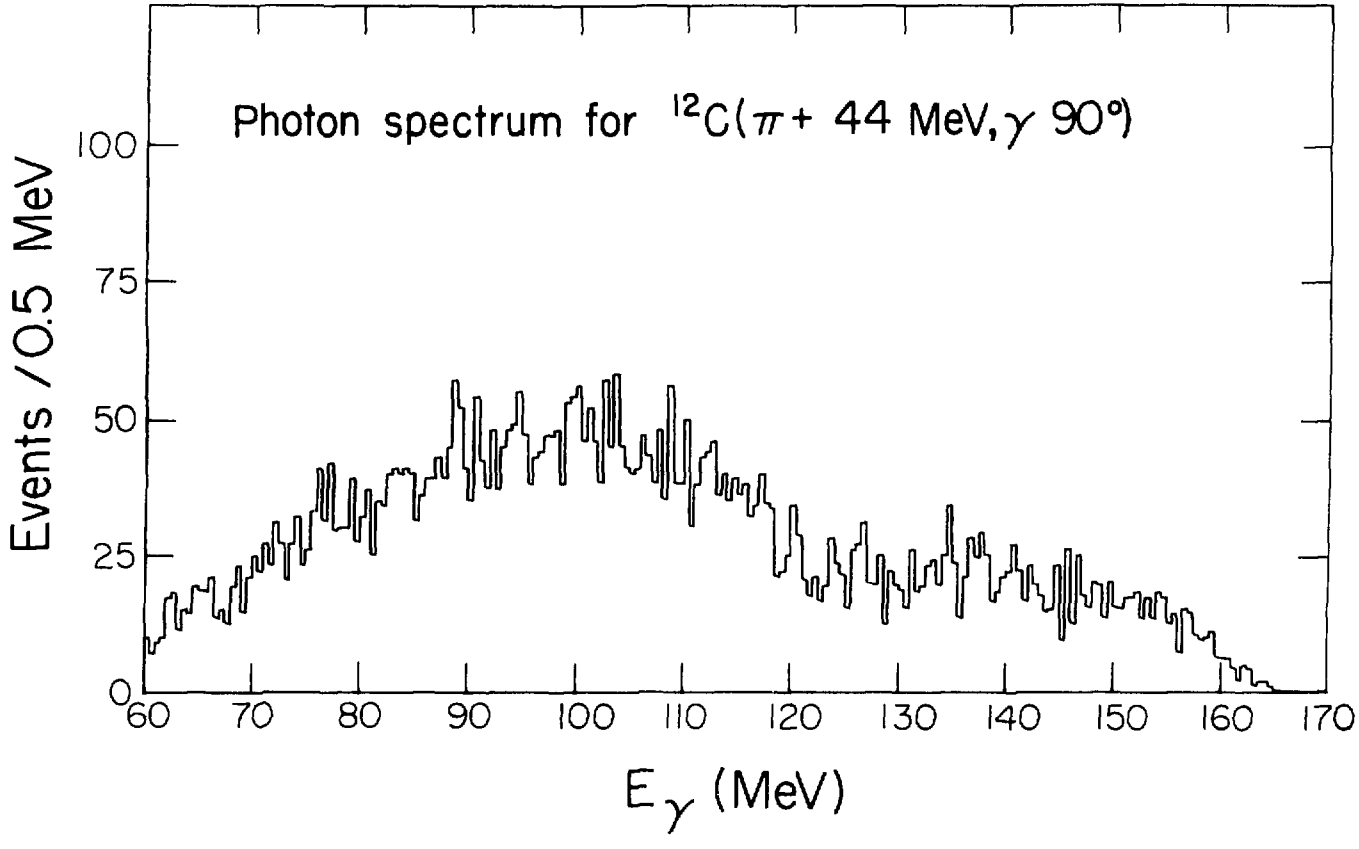

XBL806-1228

Fig. 10. Photon spectrum from capture in flight of 44 MeV π^+ by ^{12}C.

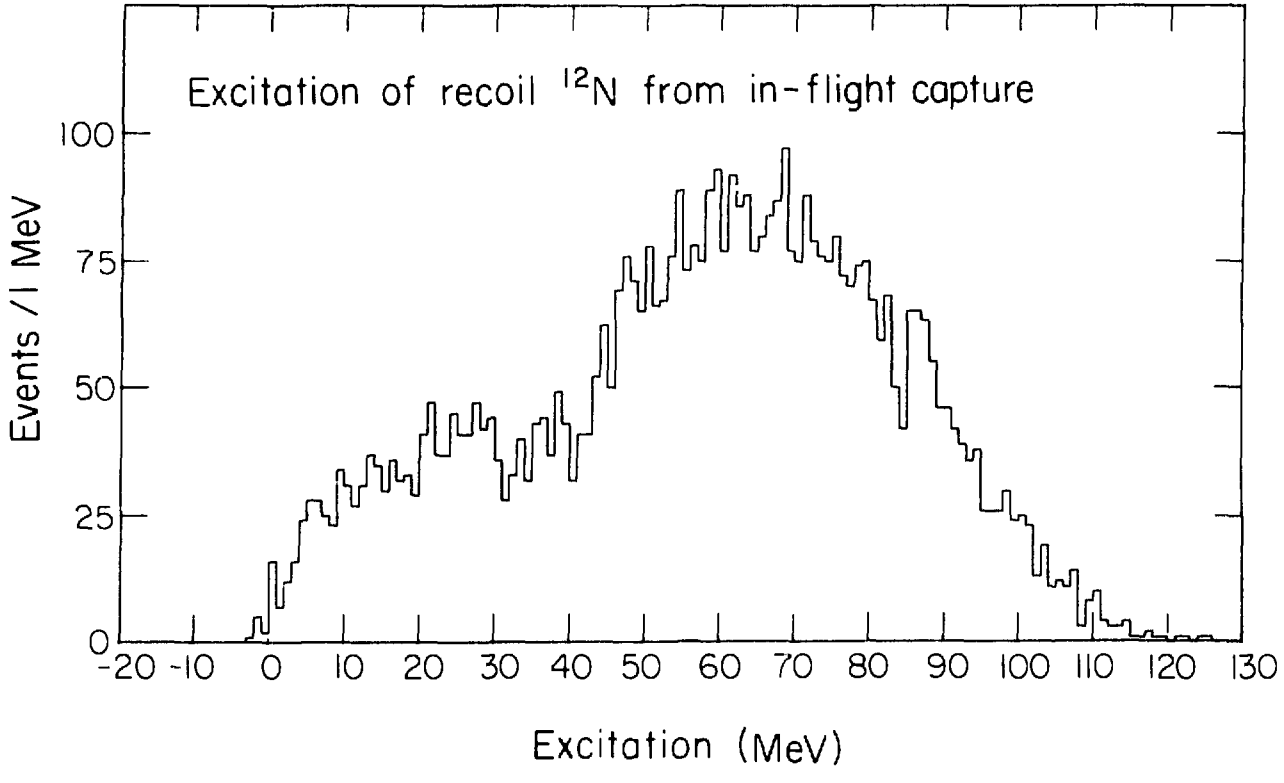

XBL 806-1314

Fig. 11. Excitation energy of recoiling ^{12}N derived from Fig. 10.

The cross section has been obtained from the pair spectrometer acceptance measured with negative pions stopping in hydrogen, and the backscattering pion flux "monitor" mentioned in Chapter III. The radiative cross section summed for photon energies above the kinematic cutoff for charge exchange at 131 MeV is 91 ± 18 microbarns/sr. The cross section including only photon energies from 141 MeV to the maximum is 55 ± 11 microbarns/sr. The resolution is rather broad, being limited by the 4.0 MeV thick target. In combination with the limited statistics, this makes the extraction of cross sections to discrete final states impossible.

A qualitative comparison with the $^{12}C(\pi^-,\gamma)$ spectrum[28] in Figure 12 shows certain similarities, as expected from isospin symmetry. Evidence of the ground state to ground state transition is observed. The prominent peaks near 5 and 7 MeV excitation in ^{12}B are reflected as a bump near 6.5 MeV excitation in ^{12}N.

Cannata *et al*[27] have calculated the cross sections and angular distributions for $^{12}C(\pi^+,\gamma)$ leading to various excited states of ^{12}N. Their calculations included only the Kroll-Ruderman term $(\vec{\sigma}\cdot\vec{\epsilon})\tau^+$ of the elementary pion capture transition operator. The pion momentum dependent terms were neglected. The matrix elements were obtained from inelastic electron scattering, parametrized in the Helm model. The predicted cross section for (π^+,γ) at 40 MeV, integrated from 0 to 22 MeV excitation in ^{12}N, is 59 b/sr. The theoretical spectrum is shown in Figure 13, convolved with the experimental lineshape, and correctly normalized to the observed spectrometer acceptance and integrated beam current. In the energy region considered, the agreement with experiment appears excellent.

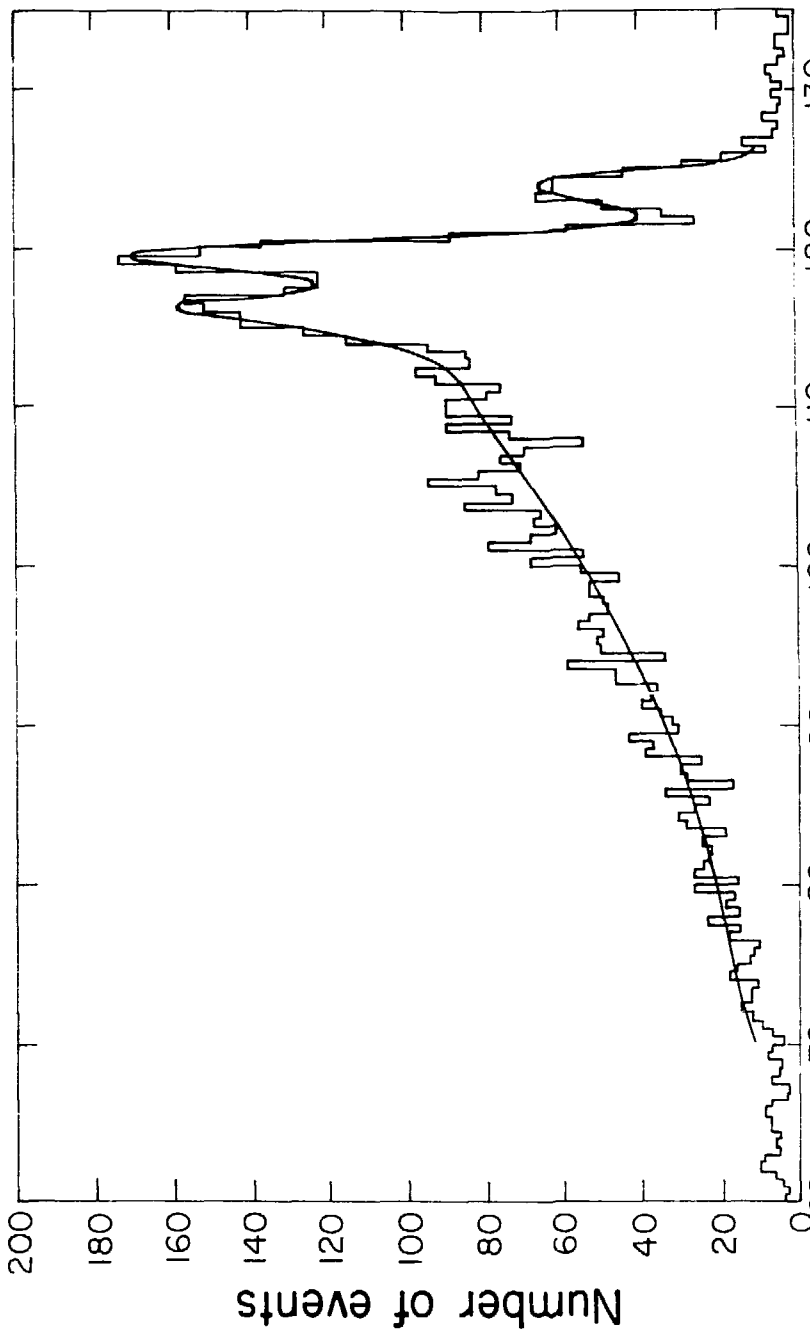

XBL806-1221

Fig. 12. Photon spectrum from radiative pi-minus capture in ^{12}C for comparison with Fig. 11. The peak near 125 MeV corresponds to the ^{12}B ground state.

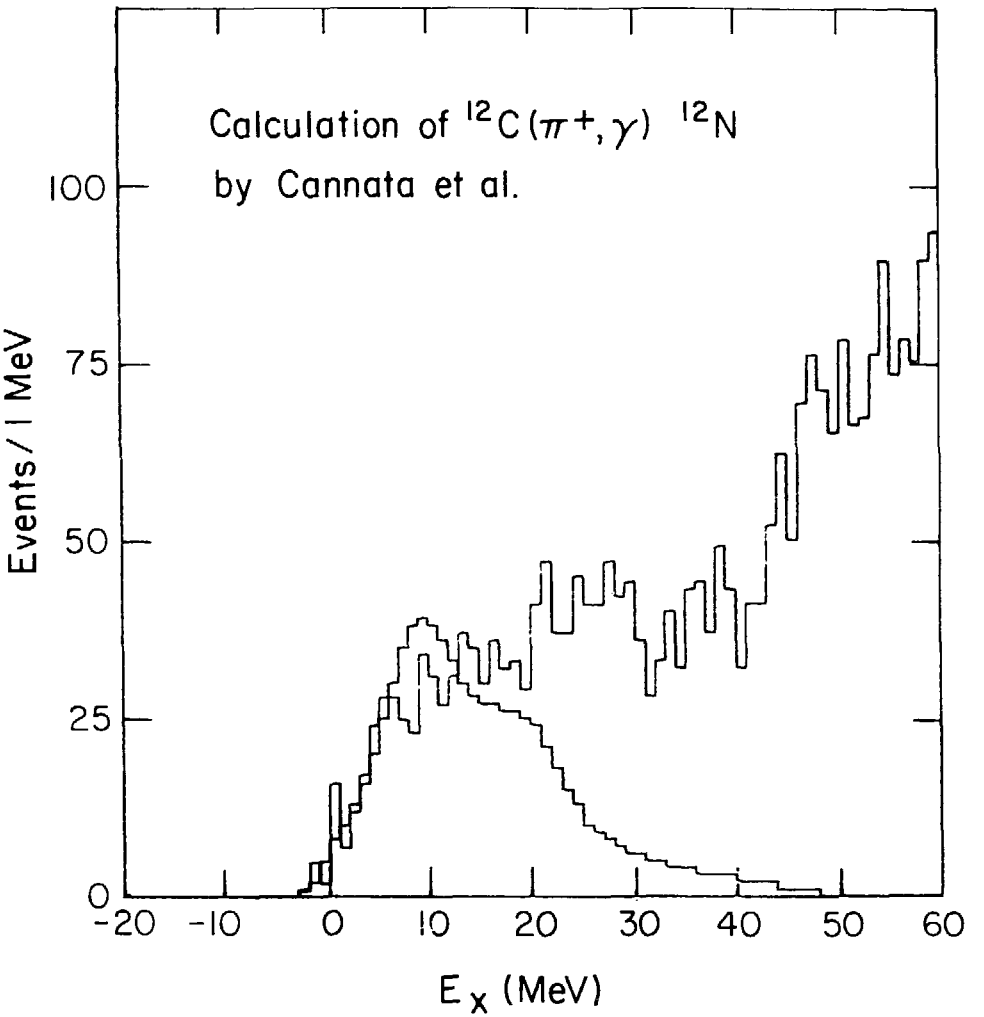

XBL 806-1226

Fig. 13. ^{12}N excitation spectrum predicted in Ref. 27 for radiative capture of 40 MeV π^+ in flight on ^{12}C, with experimental data of Fig. 11 superimposed. The curves are each properly normalized, not scaled to make them agree.

This is another example of the close correspondence of the (π,γ) reaction to electroexcitation. The agreement indicates the great potential in comparisons between these probes for studying exotic effects.

Broad enhancements appear at 25-40 MeV excitation in ^{12}N. This structure is well above the cutoffs for photons from π^0 decay at the energies attainable by charge exchange on ^{12}C (133 MeV for beam energy π^+) and on hydrogen (132 MeV). Positrons accompanying the pion beam would have an energy of only 118 MeV, too low to give bremsstrahlung radiation at the observed energy. Quasifree radiative capture could result in photons in this energy region. The expected cross section for quasifree radiative capture may be estimated from other work.

Nucleon ejection by pions has been observed in activation experiments.[76] The ^{11}C activity counted after irradiation of ^{12}C by 80 MeV positive pions was interpreted as a cross section of 44 mb for the sum of $^{12}C(\pi^+,\pi^0p)$ and $^{12}C(\pi^+,\pi^+n)$.

A similar process, $^{12}C(\pi^+,\gamma N)$, could contribute photons in the high excitation region. If the reaction is quasifree, the ratio of the reactions $^{12}C(\pi^+,\pi^0p)$ to $^{12}C(\pi^+,\gamma p)$ may be estimated from the free nucleon data for $n(\pi^+,\pi^0)p : n(\pi^+,\gamma)p$. (This is the Panofsky ratio for nonzero pion momentum.) The charge exchange cross section is given approximately by the total minus elastic cross section for π^-p scattering at 50 MeV,[77] which is 8 mb. The radiative cross section can be estimated from the $\gamma n \rightarrow \pi^-p$ cross section at 90° and invariant mass 1140 MeV,[78] multiplied by a statistical factor of two for the photon polarization. This is 0.3 mb, leading to a Panofsky ratio of ~26:1. Taking the contributions of $^{12}C(\pi^+,\pi^0p)$ and $^{12}C(\pi^+,\pi^+n)$ to the activation cross

section to be equal, one obtains $\sigma(\pi^+,\gamma p) \sim (1/2)(1/26)(44\ \text{mb})(1/4\pi) \sim$ 70 microbarns/sr. Therefore the reaction $(\pi^+,\gamma N)$ would be expected to contribute appreciably to the observed photon spectrum. (The estimate obtained above is about two times the observed cross section summed from 135-148 MeV.) The photons from this reaction might well extend below the charge exchange cutoff also.

The photon spectrum of Figure 10 also contains a large contribution from π^0 decay photons following charge exchange. A π^0 energy spectrum may be extracted from measurement of a single photon energy spectrum if the angular distribution of π^0's and the energy dependence thereof is known. These data are not available for the present reaction. An estimate of the energy-integrated cross section for charge exchange may be obtained using the spectrometer acceptance curve and accounting for the loss of ~20% of the photons below the spectrometer lower energy cutoff. The result is 1.0 ± 0.3 mb/sr. This is compatible with the value of 21 mb for the angle and energy integrated charge exchange cross section on ^{16}O measured with 50 MeV π^+.[79]

X. SUMMARY

The most important results of the present work are:

1) The rate of $^{13}C(\pi^-,\gamma)^{13}B$ g.s. is shown to be quantitatively consistent with an impulse approximation expression involving Gamov-Teller and charge quadrupole moment matrix elements measured in other experiments.

2) The strength of the (π^-,γ) transitions to higher lying excited states of ^{13}B is shown to be consistent with a giant resonance interpretation for these excitations.

3) The spin flip and orbital magnetization contributions to the isovector M1 transition in A = 20 are separately evaluated. The orbital part is shown to dominate the transition, in agreement with theoretical predictions.

4) Systematic fragmentation of the highly excited M2 resonances is observed in $^{19}F(\pi^-,\gamma)$ when compared to $^{16,18}O(\pi^-,\gamma)$ measured by others.

5) The cross section for radiative capture of π^+ at 44 MeV on ^{12}C is shown to be consistent with theoretical predictions using a simplified impulse approximation Hamiltonian and matrix elements measured in electroexcitation.

6) Evidence for quasifree radiative capture in flight is observed, with a cross section differing by a factor 2 from a very simplified estimate based on the free nucleon Panofsky ratio and $(\pi,\pi N)$ cross sections for ^{12}C.

These results contribute to the body of pre-existing work in

photopion nuclear physics in establishing these reactions as useful nuclear physics probes, and in gaining quantitative nuclear structure information unobtainable by other means. In particular, the detailed study of M1 transitions and pursuit of comparisons between radiative pion capture and inelastic electron scattering has been fruitful.

Future work should concentrate on three areas:

1) Better understanding of the M2 resonances observed in (π^-,γ) in light nuclei. The theoretical work of the Dubna group[48,52] may continue to be helpful in this regard.
2) Treatment of the meson exchange corrections in (π^-,γ), both theoretically and in the type of phenomenological analyses presented here.
3) Extension of (π,γ) measurements to the in-flight case, where momentum transfer dependence and angular dependence may provide a rich source of information on magnetic transitions in nuclei.

For the interpretation of existing pion capture at rest data, new accurate and precise measurements of the pionic total widths, in particular for the carbon isotopes, would be extremely valuable.

ACKNOWLEDGMENTS

I would like to thank my collaborators and the other people whose work has made possible the completion of the experiments upon which this thesis is based.

The collaborators on Experiment 348 were H. W. Baer, J. A. Bistirlich, C. W. Clawson, K. M. Crowe, M. Koike, J. P. Miller, S. S. Rosenblum, G. Strassner, P. Truöl, A. H. Wapstra, and W. A. Zajc.

The wire chamber electronic system was designed by the LBL Nuclear Instrumentation group under S. R. Olsen. Much of the software and software support was due to J. M. Gallup, E. Lieberman, and S. Schlaer.

This work was done under the sponsorship of the Office of Energy Research, U.S. Department of Energy, under Contract W-7405-ENG-48.

REFERENCES

1. W.K.H. Panofsky, R.L. Aamodt, and J. Hadley, Phys. Rev. 81, 565 (1951).

2. J. Spuller, D. Berghofer, M.D. Hasinoff, R. MacDonald, D.F. Measday, M. Salomon, T. Suzuki, J.-M. Poutissou, R. Poutissou, and J.K.P. Lee, Phys. Lett. 67B, 479 (1977).

3. K. Brueckner, R. Serber, and K. Watson, Phys. Rev. 81, 575 (1951).

4. H. Davies, H. Muirhead, and J.N. Woulds, Nucl. Phys. 78, 673 (1966).

5. V.I. Petrukhin and Y.D. Prokoshkin, Nucl. Phys. 66, 669 (1965).

6. J. Tiomno and J.A. Wheeler, Rev. Mod. Phys. 21, 153 (1949).

7. H. Primakoff, Rev. Mod. Phys. 31, 802 (1959).

8. J.S. Bell and L. Lovseth, Nuovo Cimento 32, 433 (1964).

9. J.R. Luyten, H.P.C. Rood, and H.A. Tolhoek, Nucl. Phys. 41, 236 (1963).

10. J. Barlow, J.C. Sens, P.J. Duke, and M.A.R. Kemp, Phys. Lett. 9, 84 (1964).

11. L.L. Foldy and J.D. Walecka, Nuovo Cimento 34, 1026 (1964).

12. A.E. Glassgold, W. Heckrotte, and K.M. Watson, Annals of Phys. 6, 1 (1959).

13. J.D. Walecka, "Giant resonances in nuclei," in Preludes to Theoretical Physics, A. De Shalit, H. Feshbach, and L. Van Hove, eds. (Wiley & Sons, New York, 1966), p. 59.

14. H. Uberall, in High Energy Physics and Nuclear Structure, S. Devons, ed. (Plenum Press, New York, 1970), p. 48.

15. J. Delorme and T.E.O. Ericson, Phys. Lett. 21, 98 (1966).

16. D.K. Anserson and J.M. Eisenberg, Phys. Lett. 22, 164 (1966).

17. F.J. Kelly and H. Überall, Nucl. Phys. A118, 302 (1968).

18. J.A. Bistirlich, K.M. Crowe, A.S.L. Parsons, P. Skarek, and P. Truöl, Phys. Rev. Lett 25, 689 (1970).

19. H.W. Baer, K.M. Crowe, and P. Truöl, "Radiative pion capture in nuclei," in Advances in Nuclear Physics, Vol. 9, M. Barranger and E. Vogt, ed. (Plenum Press, New York, 1977), pp. 207-211.

20. D. Griffiths and C.W. Kim, Phys. Rev. 173, 1584 (1968); see also other references in Ref. 19, p. 209.

21. D. Renker, W. Dahme, W. Hering, H. Panke, Č. Zupančič, J.C. Alder, B. Gabioud, C. Joseph, J.F. Loude, N. Morel, J.P. Perroud, A. Perrenoud, M.T. Tran, E. Winkelmann, G. Strassner, and P. Truöl, Phys. Rev. Lett, 41, 1279 (1978).

22. J.C. Adler, B. Gabioud, C. Joseph, J.F. Loude, N. Morel. A. Perrenoud, J.P. Perroud, M.T. Tran, B. Vaucher, E. Winkelmann, D. Renker, H. Schmitt, Č. Zupančič, H. Von Fellenberg, A. Frischknecht, F. Hoop, G. Strassner, and P. Truöl, Nucl. Instrum. Meth. 160, 93 (1979).

23. A. Perrenoud et al, "Isovector transitions in 1-p shell nuclei induced by radiative pion capture," submitted to Nuclear Physics A. See also Ref. 38.

24. B.H. Wildenthal and W. Chung, "Microscopic structure of $J^{\pi} = 1^{+}$ excitations in s-d shell nuclei," unpublished draft, 1979.

25. M. Ericson, Nucl. Phys. A335, 309 (1980).

26. Panel N-4 report, Los Alamos Workshop on Program Options in Medium Energy Physics (March 1979).

27. F. Cannata, B.A. Lamers, C.W. Lucas, N. Nagl, H. Überall, C. Werntz and F.J. Kelly, Can. J. Phys. 52, 1405 (1974).

28. J.A. Bistirlich, K.M. Crowe, A.S.L. Parsons, P. Skarek, P. Truöl, Phys. Rev. C5, 1867 (1972).

29. J.P. Perroud, in Photopion Nuclear Physics, P. Stoler, ed. (Plenum Press, New York, 1979), p. 89.

30. L.W. Fagg, W.L. Bendel, S.K. Numrich and B.T. Chertok, Phys. Rev. C1, 1137 (1970).

31. B.R. Mottelson, in Elementary Modes of Excitation in Nuclei, A. Bohr and R.A. Broglia, eds. (North Holland, Amsterdam, 1977), p. 47 ff.

32. G.E. Brown and M. Bosterli, Phys. Rev. Lett. 3, 472 (1959).

33. S.R. Olsen, F.A. Kirsten, E.P. Binnall, K.L. Lee, N.N. Bhandari and C.C. Nunnally, A Modular Multiwire Readout System for Proportional Wire Chambers, LBL-2445 (1973).

34. LBL CAMAC-MWPC interface modules 22×3680 and 22×3662, documentation of December 9, 1976.

35. M. Kellogg et al, Los Alamos Scientific Laboratory Report LA-7001-M (revised) (June 1978).

36. R.L. Burman, R.L. Fulton, M. Jakobson, Nucl. Instrum. Meth. 131, 29 (1975).

37. H. Wind, Proceedings CERN Data Processing School, CERN 72-21 (1972).

38. A. Perrenoud, Ph.D. thesis, "Etude de la capture radiative des pions negatifs au repos par les noyaux de la couche 1-p," Ecole Polytechnique Federale de Lausanne, Universite de Lausanne, Switzerland (1979) (unpublished).

39. J.C. Adler, B. Gabioud, F. Hoop, C. Joseph, J.F. Loude, H.A. Medicus, N. Morel, A. Perrenoud, J.P. Perroud, D. Renker, H. Schmitt, G. Strassner, M.T. Tran, P. Truöl, B. Vaucher, H.V. Fellenberg, E. Winkelmann and Č. Zupančič, in Meson Nuclear Physics, P.D. Barnes, R.A. Eisenstein, and L.S. Kisslinger, eds., API Proceedings #33, 624 (1976); P. Truöl, private communication.

40. N. Ohtsubo, T. Nishiyama, and M. Kawaguchi, Nucl. Phys. A224, 164 (1974), Appendices A and B. For a more detailed treatment, see Ref. 43.

41. N. Ohtsuka, Ph.D. thesis, "Radiative pion capture on ^{12}C and ^{16}O--Nuclear structure investigations by the shell model," Department of Physics, Osaka University, Japan (unpublished).

42. B.T. Chertok, C. Sheffield, J.W. Lightbody, S. Penner, D. Blum, Phys. Rev. C8, 23 (1973).

43. R.E. Marrs, E.G. Adelberger, and K.A. Snover, Phys. Rev. C16, 61 (1977).

44. F.S. Dietrich, M. Suffert, A.V. Nero and S.S. Hanna, Phys. Rev. 168, 1169 (1968).

45. L.K. Fifield, F.P. Calaprice, C.H. Zimmerman, M.J. Hurst, A. Pakkanen, T.J.M. Symons, F. Watt and K.W. Allen, Nucl. Phys. A288, 57 (1977).

46. L. Dakhno and Y. Prokoshkin, Sov. J. Nucl. Phys. 7, 351 (1968); see H.W. Baer, J.A. Bistirlich, N. deBotton, S. Cooper, K.M. Crowe, P. Truöl, and J.D. Vergados, Phys. Rev. C12, 921 (1975) for erratum.

47. C.S. Yang, E.L. Tomusiak, R.K. Grupta, and H.S. Caplan, Nucl. Phys. A162, 71 (1971).

48. H.R. Kissener, G.E. Dogotar, R.A. Eramzhyan and R.A. Sakaev, Nucl. Phys. A312, 394 (1978).

49. F. Ajzenberg-Selov, Nucl. Phys. A268, 1 (1976).

50. J.C. Bergstrom, H. Crannel, F.J. Kline, J.T. O'Brien, J.W. Lightbody, and S.P. Fivozinsky, Phys. Rev. C4, 1514 (1971).

51. J.D. Vergados, Phys. Rev. C12, 1278 (1975); see also references in 17.

52. G.E. Dogotar et al, JINR Communications E2-11275 (Dubna preprint) (1978).

53. K.W. Jones, W.R. Harris, M.T. Ellistrem, and D.E. Alburger, Phys. Rev. 186, 978 (1969).

54. R.S. Willey, Nucl. Phys. 40, 529 (1963), equations 2.24c, 2.64c (cited in Ref. 86).

55. G. Wittwer, H.-G. Clerc, and G.A. Beer, Phys. Lett. 30B, 634 (1969).

56. J. Dubach, invited talk at Los Alamos Conference on Nuclear Physics with Medium Energy Probes, January 1980; and J. Dubach and W.C. Haxton, Phys. Rev. Letts. 41, 1453 (1978).

57. M. Chemtob, M. Rho, Nucl. Phys. A163, 1 (1971).

58. D.M. Brink, Nucl. Phys. 4, 215 (1957).

59. M. Goldhaber and E. Teller, Phys. Rev. 74, 1046 (1948).

60. L.W. Fagg, Rev. Mod. Phys. 47, 683 (1975).

61. D. Kurath, Phys. Rev. 130, 1525 (1963).

62. J.W. Jury, B.L. Berman, D.D. Fall, P. Meyer, K.G. McNeill, and J.G. Woodworth, Phys. Rev. C19, 1684 (1979).

63. T. Schiff, Quantum Mechanics, 3rd edition, (McGraw-Hill, San Francisco, 1968), Eq. 44.23, p. 405, adapted to the present notation by averaging over initial m states and summing over final m states, and using Eq. B-1 of the present work.

64. S.S. Hanna, "Giant Resonances," in Proceedings of Int. Conf. on Nuclear Structure and Spectroscopy, Amsterdam, 1974, H.P. Blok and A.E.L. Dieperink, eds., Scholars' Press, Amsterdam, p. 249.

65. P. Truöl, private communication.

66. F. Azjenberg-Selov, Nucl. Phys. A300, 189 (1978).

67. W. Knupfer, H. Ender, and M.G. Huber, Abstract 5A12, 8th International Conference on High Energy Physics and Nuclear Structure, Vancouver, Canada, 1979.

68. F.P. Brady and G.A. Needham, "The n,p reaction on light N=Z nuclei," contribution to Telluride Conference, March 1979.

69. N.S.P. King, private communication.

70. Z.M. Szalata, K. Itoh, G.A. Peterson, J. Flanz, S.P. Fivozinsky, F.J. Kline, J.W. Lightbody, X.K. Maruyama, and S. Penner, Phys. Rev. C17, 435 (1978).

71. W.L. Bendel, L.W. Fagg, S.K. Numrich, E.C. Jones, and H.F. Kaiser, Phys. Rev. C3, 1821 (1971).

72. S. Maripuu and B.H. Wildenthal, Phys. Lett. 38B, 464 (1971).

73. P. Axel, D.M. Drake, S. Whetstone, and S.S. Hanna, Phys. Rev. Lett. 19, 1343 (1967).

74. M. Hasinoff, G.A. Fisher, and S.S. Hanna, Nucl. Phys. A216, 221 (1973).

75. G. Strassner, P. Truöl, J.C. Adler, B. Gabioud, C. Joseph, J.F. Loude, N. Morel, A. Perrenoud, J.P. Perroud, M.T. Tran, E. Winkelmann, W. Dahme, H. Panke, D. Renker, and H.A. Medicus, Phys. Rev. C20, 248 (1979), Section IV-1.

76. D.T. Chivers, J.J. Domingo, E.M. Rimmer, R.C. Witcomb, B.W. Allardyce, and N.W. Tanner, Phys. Lett. 26B, 573 (1968).

77. W. Locke and D.F. Measday, Intermediate Energy Nuclear Physics, (Methuen & Co., London, 1970), p. 97.

78. J.M. Laget, Nucl. Phys. A335, 267 (1980), Fig. 8.

79. R.P. Redwine, private communication.

80. W.W. Sapp, M. Eckhouse, G.H. Miller, R.E. Welsh, Phys. Rev. C5, 690 (1972).

81. G. Backenstoss, Ann. Rev. Nucl. Sci. 20, 467 (1970).

82. L. Tauscher, Exotic Atoms, First course of the International School of Physics of Exotic Atoms, Erice, 1977, G. Fiorentini and G. Torelli, eds. (Servizio Documentazione dei Laboratori Nazionali di Frascati, 1977), p. 145.

83. A. Olin, G.A. Beer, D.A. Bryman, M.S. Dixit, J.A. MacDonald, G.R. Mason, R.M. Pearce, and P.R. Poffenberger, Nucl. Phys. A312, 361 (1978).

84. A.L. Edmonds, Angular Momentum in Quantum Mechanics (Princeton University Press, Princeton, N.J., 1974).

85. W. Maguire and C. Werntz, Nucl. Phys. A205, 211 (1973).

86. L. Foldy and J. Walecka, Phys. Rev. 140B, 1339 (1965), Eq. (1b). The convention $t - |p\rangle = |n\rangle$ is used in this reference, but all other conventions are the same as the presen work.

87. J.D. Jackson, Classical Electrodynamics, 2nd ed. (Wiley & Sons, New York, 1975), pp. 104 and 741.

88. I.S. Gradshteyn and I.M. Ryzhik, Tables of Integrals, Series and Products (Academic Press, New York, 1965), formula 6.631·10, p. 718.

89. D. Kurath, Phys. Rev. 134, B1025 (1964).

90. J. Zofka and G. Ripka, Nucl. Phys. A168, 65 (1971).

APPENDIX A

PIONIC ATOM DATA AND NORMALIZATION DATA

This section contains the target thicknesses, detailed normalization data, and the pionic atom data used in the present work. The sources of the pionic atom data are also given.

TABLE A-1. Target thicknesses and CH_2 equivalents.

Target	Thickness (inches)	g/cm^2	dE/dx MeV/g/cm^2	CH_2 equivalent (inches)
Liquid hydrogen	0.625	0.112	4.12	0.093
^{13}C	0.75	0.528	1.78	0.188
Liquid Ne	0.625	0.754	1.73	0.54
^{90}Zr	0.125	2.48	1.36	1.72
^{12}C	0.75	3.49	1.78	1.23
(CH_2) 0.94 g/cm^3	--	--	(2.09)	--
^{12}C for in-flight	0.263	1.35	1.78	0.474
LiF	0.551	3.74	1.68	1.18
CF_2	0.50	2.89	1.72	1.01

TABLE A-2. Experimental quantities used in normalization.

Target	T	M_T	$(\pi_S/\pi_{in})_T$	$(\pi_{in}/M)_T$	U
Liquid hydrogen	769	$2.15 \cdot 10^5$	0.10 ± 0.005	$(3.032 \pm 0.15) \cdot 10^4$	1.
^{13}C	250	$9.045 \cdot 10^5$	0.17 ± 0.009	$(3.96 \pm 0.20) \cdot 10^4$	1.111 ± 0.044
Liquid Ne	225	$1.72 \cdot 10^5$	0.45 ± 0.04	$(5.42 \pm 0.27) \cdot 10^4$	1.091 ± 0.050
^{90}Zr	160	$4.73 \cdot 10^5$	0.30 ± 0.05	$(2.74 \pm 0.14) \cdot 10^4$	1.125 ± 0.053
^{12}C	949	$8.26 \cdot 10^5$	0.82 ± 0.04	$(3.42 \pm 0.17) \cdot 10^4$	1.096 ± 0.046
^{12}C in-flight	836	--	--	--	--
LiF	643	$2.50 \cdot 10^5$	0.66 ± 0.05	$(5.41 \pm 0.27) \cdot 10^4$	1.104 ± 0.048
CF_2	862	$9.05 \cdot 10^5$	0.59 ± 0.04	$(3.30 \pm 0.17) \cdot 10^4$	1.109 ± 0.048

TABLE A-3. Pionic atom widths and capture schedules.

Target	ω_p	ω_s	Γ_{2p}, eV	Γ_{1s}, keV
^{13}C	0.92 ± 0.03	0.08 ± 0.03	1.95 ± 0.6	3.06 ± 0.33
^{20}Ne	0.95 ± 0.05	0.05 ± 0.05	20.0 ± 7.0	14.5 ± 3.0
^{90}Zr	--	--	Γ_{3d} = 0.5±0.3 keV	--
^{19}F	0.96 ± 0.01	0.041±0.01	10.12 ± 0.74	7.0 ± 2.5
^{12}C	0.92 ± 0.03	0.08 ± 0.03	1.95 ± 0.6	3.06 ± 0.33

Sources for Table A-3

^{13}C:

ω_p,ω_s from Table II, Ref. 80 for ^{12}C.

Γ_{2p} is the optical model fit value for ^{12}C from Figure 3 of Ref. 80. The numerical value was obtained by scaling the ordinate of the experimental value 2.6 ± 0.9.

Γ_{1s} is a weighted average of the ^{12}C values from Table 3, Ref. 81.

The use of ^{12}C values is reasonable in the absence of ^{13}C data and in view of the observation that there is no significant influence of a missing or additional neutron on the level widths (Ref. 82, p.150).

^{20}Ne:

ω_s,ω_p are estimated from the values given in Ref. 81 for ^{19}F and ^{23}Na. The values are quite insensitive to Z.

Γ_{2p} is interpolated from Figure 8 of Ref. 81. The uncertainty is estimated from the spread of ^{16}O values reported in Ref. 75.

Γ_{1s} is from Table 3, Ref. 82.

^{90}Zr:

Γ_{3d} has been measured for neighboring $^{89}_{39}Y$(0.8 ± 0.6 keV), $^{93}_{41}Nb$ (0.52 ± 0.1 keV), and $^{96}_{42}Mo$(0.56 ± 0.10 keV). The value given is interpolated from these, which appear in Table 4, Ref. 81.

^{19}F:

ω_s and ω_p are from Table 2, Ref. 83.

Γ_{2p} is the average value from Table 3, Ref. 81; Γ_{1s} from Ref. 83.

^{12}C:

See ^{13}C above.

APPENDIX B.

REFERENCES FOR THEORETICAL FORMULAE

General Notation

1. Physical Quantities

M_π = charged pion mass = 139.57 MeV

M = nucleon effective mass = 1/12 (^{12}C mass) = 931.48 MeV

M_A = target nucleus mass = $A*M+\Delta$

g_s^p = proton spin g-factor = 5.5857 nuclear magnetons

g_ℓ^p = proton orbital g-factor
= +1 nuclear magnetons

g_s^n = neutron/spin g-factor = 0

g_ℓ^n = neutron orbital g-factor = -3.8260 nuclear magnetons

$k=|\vec{k}|=|\vec{p}|/\hbar$ = photon wave number of 3-momentum

$q=|\vec{q}|$ = 3-momentum transfer

$a_\pi = \frac{\hbar^2 c^2}{ZM_\pi e^2}$ = pionic Bohr radius for nuclear charge Z

$\phi_{n\ell}$ = pion wave function in combined Coulomb and optical potential of nucleus

$\phi^H_{n\ell}$ = hydrogenic pion wave function in Coulomb potential only

$C_{n\ell}$ = pion wave function distortion factor, see Ref. 19, p.196

$$\equiv \frac{|\langle J_f|r^{-\ell}\phi_{n\ell}|J_i\rangle|^2}{|\langle J_f|r^{-\ell}\phi^H_{n\ell}|J_i\rangle|^2}$$

2. Operators and Matrix Elements

$\langle J_1M_1J_2M_2|JM\rangle$ = Clebsch Gordan coefficients, phase convention of Ref. 84

$W(abcd;ef)$ = Racah coefficients, defined in terms of 6-j symbols in Ref. 84

$\vec{\sigma} = 2\vec{S}$ = nucleon Pauli spin operator

$r_n = |\vec{r}_n|$ = radial coordinate of the nth nucleon

$\langle J_f|$ = final nuclear state with total angular momentum J_f (other quantum numbers suppressed)

$\langle J_f \| T_J \| J_i \rangle$ = reduced transition matrix element of tensor operator T_{JM}, convention of Refs. 40 and 41

$$= \frac{\sqrt{2J_f+1}}{\langle J_i M_i JM | J_f M_f \rangle} \langle J_f M_f | T_{JM} | J_i M_i \rangle, \quad \text{also}$$

$$|\langle J_f \| T_J \| J_i \rangle|^2 = (2J_i+1) \sum_{m,m_f} |\langle J_f M_f | T_{JM} | J_i M_i \rangle|^2 \qquad (B\text{-}1)$$

t_+ = isospin raising operator which turns protons into neutrons (nuclear physics convention)

$t_+|p\rangle = |n\rangle$

$$[T_k \otimes Y_\ell]_{Jm} = \sum_{m_k, m_\ell} \langle k m_k \ell m_\ell | Jm \rangle \, T_{k m_k} Y_{\ell m_\ell}$$

$R_{LJ} = \langle J_f \| [\sigma \otimes Y_L]^J t_+ \| J_i \rangle$ $L_{LJ} = \langle J_f \| [L \otimes Y_L]^J t_+ \| J_i \rangle$ $Y_L = \langle J_f \| Y_L \| J_i \rangle$

$j_\ell(x)$ = spherical Bessel function of order ℓ

ℓ_π = pion orbital angular momentum

$\vec{\varepsilon}$ = photon polarization 3-vector

Transition Rate for Radiative Pion Capture

Formulae are reproduced from section 2.3 and Appendix 2 of Ref. 41. These give the transition rate explicitly in terms of matrix elements of single nucleon operators.

The pion radiative capture rate for capture on state $|J_i\rangle$ leading to $\langle J_f|$ from pionic orbital $\phi_{n\ell_\pi}$ with orbital angular momentum ℓ_π is[41,42]

$$W = \frac{16\pi^2 k}{M_\pi (2J_i+1)(2\ell_\pi+1)} \sum_{J,L} \left| \langle J_f | \sum_{n=1}^{A} M_A(J,L,\ell_\pi;r_n) | J_i \rangle \right|^2$$

$$+ \left| \langle J_f | \sum_{n=1}^{A} M_b(J,L,\ell_\pi;r_n) | J_i \rangle \right|^2 .$$

Some authors[85] introduce "reduced masses"

$$\mu_\pi = \left(\frac{1}{M_\pi} + \frac{1}{M}\right)^{-1} \quad , \qquad K = \left(\frac{1}{k} + \frac{1}{M_A}\right)^{-1}$$

to replace M_π and k in the above expressions. In the present work, the factor μ_π/M_π has been put into the pion-nucleon interaction coefficients A,B,C,D, and the factor K/k has been ignored, following Ohtsuka.[41]

The operators M_a and M_b are determined from the elementary process of pion photoproduction on the nucleon. These operators are given by Ohtsuka [Eqs. 2.33a and Appendix 2 in Ref. 41] in terms of single nucleon operators, Clebsch-Gordan coefficients and Racah coefficients. The terms relevant to even parity transitions in the 1-p shell have been worked out by Perrenoud.[38] Those of Perrenoud's terms that are relevant to the present work have been checked and are displayed in Appendix C. The terms for the transitions $J = 0^+ \rightarrow 2^-$ and $1/2^- \rightarrow 5/2^+$ have been calculated and are also shown in Appendix C.

These expressions have been reduced by using harmonic oscillator radial wave functions to evaluate the radial integrals, inserting numerical values of the pion-nucleon interaction coefficients, and using hydrogenic wave functions multiplied by "distortion factors"[19] the the pions. Numerical expressions are thereby obtained for the radiative capture rate from particular pionic atom orbitals to particular nuclear states, in terms of the spin-angular matrix elements Y_{LJ} and R_{LJ}. The branching ratios are then calculated by dividing these rates by the total disappearance rates (pionic atom widths) shown in Table A-3 and summing over capture orbitals with weights given by the capture probabilities $\omega_{n\ell}$ shown in the same table. The final expressions give the branching ratios in terms of the spin-angular matrix elements alone.

Formula for Beta Decay

For the allowed Gamow-Teller beta decay taking $J^\pi = 0^+ \to 1^+$, Foldy and Walecka[86] give

$$ft_{\frac{1}{2}} = \frac{2\pi^3 \ln(2)}{|GF_A^\beta|^2 m_e^5 \left(\frac{1}{3}\right) |\langle 0^+ \| \sum_{i=1}^{A} t_i^- \sigma_i \| 1^+ \rangle|^2} .$$

To generalize this to other nuclear spins, note that the factor 1/3 results from the $1/(2J_i+1)$ in Edmond's definition of the reduced matrix element. The numerical value of $|G|^2 m_e^5$ is $7.11 \cdot 10^{-3}$ sec^{-1} [Ref. 86, Eq. 7], and $F_A^\beta = 1.23$. These values give $\frac{1}{2}|\langle \frac{1}{2}^+ \| (1 + F_A^\beta \sigma) t^- \| \frac{1}{2}^+ \rangle|^2 = 5.64 \pm 0.09$ for neutron decay, where the Fermi matrix element has been included. To verify that the convention for the reduced matrix element is the same in the present work and in Ref. 86, one may calculate the matrix element for neutron decay in the present notation from Eq. (B-1) above:

$$\langle \tfrac{1}{2}^+ \| t^- 1 \| \tfrac{1}{2}^+ \rangle = \frac{\sqrt{2(\frac{1}{2})+1}}{\langle \frac{1}{2} M_i 00 | \frac{1}{2} M_f \rangle} \langle \tfrac{1}{2} M_f | 1 | \tfrac{1}{2} M_i \rangle = \sqrt{2}$$

$$\langle \tfrac{1}{2}^+ \| t^- \sigma \| \tfrac{1}{2}^+ \rangle = \frac{\sqrt{2}}{\langle \frac{1}{2} M_i | 0 | \frac{1}{2} M_f \rangle} \langle \tfrac{1}{2} M_f | \sigma_z | \tfrac{1}{2} M_i \rangle = \frac{\sqrt{2}}{\frac{1}{\sqrt{3}}} = \sqrt{6}$$

$$\tfrac{1}{2}(\sqrt{2})^2 + (1.23)^2 (\sqrt{6})^2 = 5.539 .$$

Therefore one may insert $[\vec{\sigma} \times Y_0]^1 = \frac{1}{\sqrt{4\pi}} \vec{\sigma}$ into the first formula of this section, along with the constants given above, to obtain:

$$ft_{\frac{1}{2}} = 318 \frac{2J+1}{|\langle J_f \| [\sigma \otimes Y_0]^1 t_- \| J_i \rangle|^2} .$$

Formulae for Electron Scattering

The radiative pion capture operator contains spin-dependent terms similar to those involved in the transverse part of electron scattering. Inelastic electron scattering at 180° is purely transverse and has rapidly developed in the last few years[60] into a fine nuclear structure probe. Comparison with radiative pion capture can give additional information on transition mechanisms. Therefore formulae relating to measured (e,e') cross sections are given here.

The inelastic scattering cross section for an isovector transition of pure magnetic multipole order ℓ is[54]:

$$\frac{d\sigma}{d\Omega} = \frac{\pi}{\ell(\ell+1)} \frac{1}{2J_i+1} \frac{k_f^2 q^2}{k_i^4} \frac{e^4}{4M^2} |\langle J_f \| S_\ell^{mag} t_3 \| J_i \rangle|^2$$

$$S_\ell^{mag} = \sum_{i=1}^{A} \left[(g_p^\ell - g_n^\ell) \left\{ \sqrt{\frac{\ell+1}{2\ell+1}}\, j_{\ell+1}(qr_i)\, [L \otimes Y_{\ell+1}]^\ell \right.\right.$$

$$\left.\left. + \sqrt{\frac{\ell}{2\ell+1}}\, j_{\ell-1}(qr_i) [L \otimes Y_{\ell-1}]^\ell \right\} + \frac{g_p^S - g_n^S}{4} \right.$$

$$\times \left\{ -\ell \sqrt{\frac{\ell+1}{2\ell+1}}\, j_{\ell+1}(qr_i)\, [\sigma \otimes Y_{\ell+1}]^\ell \right.$$

$$\left.\left. + (\ell+1) \sqrt{\frac{\ell}{2\ell+1}}\, j_{\ell-1}(qr_i)\, [\sigma \otimes Y_{\ell-1}]^\ell \right\} \right]$$

$\hbar = c = 1$, k_i = incident electron wave number

k_f = final electron wave number

For electric transitions (or transitions in which both electric and magnetic multipoles contribute), contributions must be included from

$$S_\ell^{E\ell} = \sum_{i=1}^{A} \left[(g_p^\ell - g_n^\ell) \left\{ - \frac{km_p}{q} \left[(\ell+1) j_\ell(qr) - qr j_{\ell+1}(qr) \right] \right.\right.$$

$$\left.\left. + \left[j_\ell(qr) r \frac{d}{dr} - \frac{d}{dr} r j_\ell(qr) \right] [Y_\ell]^\ell \right\} + \frac{g_p^S - g_n^S}{4} \sqrt{\ell(\ell+1)}\, j_\ell\, [\sigma \times Y_\ell]^\ell \right]$$

Experimentalists often quote the results of electron scattering experiments in terms of Γ_0. This is the radiative width for decay of the upper state seen in inelastic scattering to the ground state, calculated with the measured inelastic scattering matrix elements. It is given by the limit $q \to E_x$ of the transition operator S_ℓ^{mag}, with the appropriate kinematical factors. For an M1 decay, the result is given in Eq. (21) of Ref. 44. In the present notation this reads

$$\Gamma_0 = \frac{1}{2J_i+1} \left(\frac{\langle T_f T_f^3 10 | T_i T_{i3} \rangle_\gamma}{\langle T_f T_f^3 1-1 | T_i T_{i3} \rangle_\beta} \right)^2 E_{fi}\, e^2 \left(\frac{q}{2M} \right)^2 \frac{8\pi}{3} \left| L_{01} + \frac{g_p - g_n}{2} R_{01} \right|^2$$

(The first two factors are needed to generalize from the $J = 1^+ \to 0^+$, $T = 1 \to 0$ case considered in Ref. 86 to arbitrary J and T. See also Ref. 44 for an application of this formula to ^{13}C. The CG coefficients are those for the J_i, J_f of the M1 gamma decay and the analog beta decay from which R_{01} is determined.)

APPENDIX C.

EXPLICIT FORMS OF RADIATIVE PION CAPTURE OPERATORS FOR $\Delta J^{\pi} = 0^{+} \to 1^{+}$, $1/2^{-} \to 3/2^{+}$, $1/2^{-} \to 5/2^{+}$

The parity of $M_a(J,L,\ell_\pi)$ is $(-)^{L+\ell_\pi+1}$, and that of $M_b(J,L,\ell_\pi)$ is $(-)^{L+\ell_\pi}$. Therefore the following operators are relevant for $\Delta J^{\pi} = 1^{+}$ transitions from $0^{+} \to 1^{+}$ or $1/2^{-} \to 3/2^{-}$:

$$M_b(1,1,1) = \frac{K_{2p}}{\sqrt{4\pi}}\Big[(-Arj_1 + k(C-B)j_0)\ t_+[\sigma\otimes Y_0]^1 + \frac{1}{\sqrt{2}}(-Arj_1 + k(B+2C)j_2)\ t_+[\sigma\otimes Y_2]^1\Big]$$

$$M_b(2,1,1) = \frac{K_{2p}}{\sqrt{4\pi}}\left[\frac{3}{\sqrt{10}}(-Arj_1 + Bkj_2)\ t_+[\sigma\otimes Y_2]^2 + \sqrt{\frac{3}{5}}\ Dkj_2\ t_+Y_2\right]$$

$$M_a(1,2,1) = \left[\frac{K_{2p}}{\sqrt{4\pi}}(Arj_1 + k(B+C)j_0)\ t_+[\sigma\otimes Y_0]^1 - 3\sqrt{2}\left(\frac{rA}{5}\left(j_3 + \frac{j_1}{6}\right) + \frac{k}{3}\left(\frac{B}{2} - C\right)j_2\right)t_+[\sigma\otimes Y_2]\right]^1$$

$$M_a(2,2,1) = \frac{K_{2p}}{\sqrt{4\pi}}\sqrt{3}\ Dkj_2\ t_+Y_2$$

$$M_b(2,2,0) = \frac{K_{1s}}{\sqrt{4\pi}}\ Aj_2[\sigma\otimes Y_2]^2\ t_+$$

$$M_b(2,3,1) = \frac{K_{2p}}{\sqrt{4\pi}}\sqrt{\frac{8}{5}}(Arj_3 + kBj_2)\ t_+[\sigma\otimes Y_2]^2$$

$$M_a(1,1,0) = \frac{K_{1s}}{\sqrt{4\pi}}A\left(\frac{1}{\sqrt{3}}\ j_2[\sigma\otimes Y_2]^1\ t_+ - \sqrt{\frac{2}{3}}\ j_0[\sigma\otimes Y_0]^1\ t^+\right)$$

The operators for $\Delta J^{\pi} = 2^-$ transitions from $0^+ \to 2^-$ or $1/2^- \to 5/2^+$ are:

$$M_a(2,1,1) = \frac{K_{2p}}{\sqrt{4\pi}} \sqrt{\frac{2}{3}} \left[\left(-Ar\left(j_0 + \frac{j_2}{10}\right) + \frac{9}{10} kj_1 \left(B - \frac{2}{3} C\right) \right) t_+ [\sigma \otimes Y_1]^2 \right.$$
$$\left. + \frac{3}{5} \left(Arj_2 - kj_3 \left(B - \frac{C}{6}\right) \right) t_+ [\sigma \otimes Y_3]^2 \right]$$

$$M_a(2,3,1) = \frac{K_{2p}}{\sqrt{4\pi}} \left[\frac{2\sqrt{6}}{5} \left(Arj_2 + j_1 k(B+C)\right) [\sigma \otimes Y_1]^2 \right.$$
$$\left. + \frac{1}{7} \left(-6Ar \left(j_4 + \frac{1}{15} j_2\right) + \frac{43}{5} Ckj_3 \right) t_+ [\sigma \otimes Y_3]^2 \right]$$

$$M_a(3,3,1) = \frac{K_{2p}}{\sqrt{4\pi}} \left(\left(\frac{2}{7} Ar\left(\frac{3}{4} j_4 - j_2\right) - \frac{11}{12} Ckj_3 - \frac{1}{2} Bkj_3 \right) t_+ [\sigma \otimes Y_1]^3 \right.$$
$$\left. - \sqrt{3} \; Dkj_3 \; t_+ Y_3 \right)$$

$$M_b(2,2,1) = \frac{K_{2p}}{\sqrt{4\pi}} \left(\sqrt{\frac{3}{2 \cdot 5}} \left(-Arj_2 + kj_1 (2C - B) \right) t_+ [\sigma \otimes Y_1]^2 \right.$$
$$\left. + \frac{1}{\sqrt{5}} \left(-Arj_2 + 3kj_3 \left(\frac{B}{3} + C\right) \right) t_+ [\sigma \otimes Y_3]^2 \right)$$

$$M_b(3,2,1) = \frac{K_{2p}}{\sqrt{4\pi}} \frac{2\sqrt{2}}{7} \left[(-Arj_2 + kj_3 B) \; t_+ [\sigma \otimes Y_3]^3 + \sqrt{\frac{3}{2}} \; Dk \; t_+ Y_3 \right]$$

$$M_b(3,4,1) = \frac{K_{2p}}{\sqrt{4\pi}} \sqrt{\frac{5}{7}} \left[\frac{3}{2} \left(Arj_4 - Bkj_3\right) t_+ [\sigma \otimes Y_3]^3 - \sqrt{3} \; Dj_3 \; t_+ Y_3 \right]$$

In the above expressions, the arguments of the Bessel functions are always kr. The coefficients A-D are equal to the C_i of Ohtsuka[41]:

$$A = C_1 \quad , \qquad B = C_3 \quad , \qquad C = C_4 \quad , \qquad D = C_2 \quad .$$

The coefficients A-D defined in this way differ from the "recommended" set of Ref. 19. The values used here are ($\hbar = c = 1$).

$$A = -3.68 \cdot 10^{-2}\, M_\pi^{-1} \quad , \qquad B = +0.86 \cdot 10^{-2}\, M_\pi^{-3} \quad ,$$

$$C = -4.26 \cdot 10^{-2}\, M_\pi^{-3} \quad , \qquad D = -1.61 \cdot 10^{-2}\, M_\pi^{-3} \quad .$$

The constants K_{1s} and K_{2p} are given by

$$K_{1s} = 2\sqrt{C_{1s}}\; a_\pi^{-3/2} \quad , \qquad K_{2p} = \frac{1}{2\sqrt{6}}\sqrt{C_{2p}}\; a_\pi^{-5/2} \quad ,$$

$$a = \frac{1 + \frac{M_\pi}{M_A}}{M_\pi \alpha Z} \quad , \qquad C_{1s}, C_{2p} = \text{distortion factors defined in Appendix A} \; .$$

APPENDIX D.

RADIAL MATRIX ELEMENTS FOR RADIATIVE PION CAPTURE

The normalized n = 1 harmonic oscillator wave functions are

$$\psi = \sqrt{\frac{4}{3r_0^3}}\sqrt{\frac{2}{\sqrt{\pi}}}\,\frac{r}{r_0}\,\exp\left(-\tfrac{1}{2}\,\frac{r^2}{r_0^2}\right) \quad .$$

In spherical coordinates one then has the radial matrix element

$$\langle\psi|f(r)|\psi\rangle = \frac{8}{3r_0^5\sqrt{\pi}}\int_0^\infty e^{-(r/r_0)^2}\, r^4\, f(r)\, dr \quad .$$

Here r_0 is related to the usual harmonic oscillator parameter ω of $U = \tfrac{1}{2}M\omega^2 r^2$ by $r_0 = \sqrt{\hbar/M\omega}$.

Let $f(x) = r^k j_\ell(qx) = r^k\sqrt{\pi/2qx}\; J_{\ell+\frac{1}{2}}(qx)$. Here j_ℓ are spherical Bessel functions and J_ℓ are Bessel functions of the first kind, as defined in, e.g., Ref. 87. Then,

$$\langle\psi|r^k j_\ell(qr)|\psi\rangle = \frac{4\sqrt{2}}{3r_0^5\sqrt{q}}\int_0^\infty J_{\ell+\frac{1}{2}}(qr)\, r^{k+4-\frac{1}{2}}\, e^{-(r/r_0)^2}\, dr \quad .$$

Let $t = r/r_0$, obtain

$$\langle\psi|r^k j_\ell(qr)|\psi\rangle = \frac{4\sqrt{2}}{3r_0^5\sqrt{q}}\, r^{k+4-\frac{1}{2}}\int_0^\infty t^{k+4-\frac{1}{2}}\, e^{-t}\, J_{\ell+\frac{1}{2}}(r_0 qt)\, dt \quad .$$

This integral is tabulated by Gradshteyn, Ref. 88.

$$\int_0^\infty e^{-t^2}\, t^{2n+\mu+1}\, J_\mu(2t\sqrt{z})\, dt = \frac{n!}{2}\, e^{-z}\, z^{\mu/2}\, L_n^\mu(z) \quad ,$$

with

$$L_n^\mu(z) \equiv \sum_{m=0}^{n} (-)^m \binom{n+\mu}{n-m}\frac{1}{m!}\, z^m \quad .$$

Using the above, one obtains

$$\langle\psi|j_0|\psi\rangle = \frac{2}{3}\, e^{-\left(\frac{r_0 q}{2}\right)^2}\left(\frac{3}{2} - \left(\frac{r_0 q}{2}\right)^2\right) ,$$

$$\langle\psi|rj_1|\psi\rangle = \frac{2}{3}\, e^{-\left(\frac{r_0 q}{2}\right)^2} r_0^2\, \frac{q}{2}\left(\frac{5}{2} - \left(\frac{r_0 q}{2}\right)^2\right),$$

$$\langle\psi|j_2|\psi\rangle = \frac{2}{3}\, e^{-\left(\frac{r_0 q}{2}\right)^2}\left(\frac{r_0 q}{2}\right)^2 ,$$

$$\langle\psi|rj_3|\psi\rangle = \frac{2}{3}\, e^{-\left(\frac{r_0 q}{2}\right)^2} r_0^4\left(\frac{q}{2}\right)^3 .$$

The first and third of these are given explicitly in Ref. 89. Some general formulas are given in Ref. 54.

Note that these n = 1 matrix elements are appropriate also for $1d_{3/2}$ and $1d_{5/2}$ shell nucleons, but not for $2s_{1/2}$ nucleons.

The oscillator parameters used were

^{13}C , $r_0 = 1.881 \pm 0.053$ fm, Ref. 42 for ^{12}C inelastic (e,e')

^{20}Ne, $r_0 = 1.834$ fm, Ref. 90.

The deformation of ^{20}Ne has been ignored in this treatment; the value of r_0 represents an average.

In the cases of $\langle j_1\rangle$, $\langle rj_2\rangle$, $\langle rj_0\rangle$, these analytic forms fail. The integrations were carried out by Simpson's Rule with 15 points.

APPENDIX E.

DECOMPOSITION OF SPECTRA FROM COMPOSITE TARGETS

This shows how to obtain the ^{19}F spectrum from ^{Nat}LiF and CF_2 spectra, knowing only the ^{Nat}Li and ^{12}C spectra.

Define

$$f_i = x_i + \beta y_i \qquad \text{(E-1)}$$

$$g_i = \xi x_i + \delta z_i \qquad \text{(E-2)}$$

where f_i = number of events in i^{th} bin of LiF spectrum,

g_i = number of events in i^{th} bin of CF_2 spectrum,

x_i = number of events in i^{th} bin of LiF spectrum due to capture on ^{19}F (to be determined),

y_i = number of events in i^{th} bin of an arbitrarily normalized ^{Nat}Li spectrum (known),

z_i = number of events in i^{th} bin of an arbitrarily normalized ^{12}C spectrum (known),

ξ, β, δ = parameters to be determined.

Combining Eqs. (E-1) and (E-2) one obtains

$$f_i = \beta y_i + \alpha g_i - \gamma z_i \quad , \qquad \text{(E-3)}$$

with

$$\alpha \equiv \frac{1}{\xi} \quad , \qquad \gamma \equiv \frac{\delta}{\xi} \quad .$$

The difference between the measured F_i and the one given by Eq. (E-3) is

$$\chi^2 = \sum_i (F_i - \beta y_i - \alpha g_i + \gamma z_i)^2 \, w_i \quad ,$$

with

$$w_i = \frac{1}{F_i} \quad .$$

Differentiating this expression with respect to each of the parameters α, β, γ in turn, and setting the derivatives equal to zero, one obtains a system of linear equations for the parameter values which make χ^2 stationary:

$$\beta \sum_i y_i^2 w_i + \alpha \sum_i g_i w_i y_i - \gamma \sum_i z_i w_i y_i = \sum_i y_i$$

$$\beta \sum_i y_i w_i g_i + \alpha \sum_i g_i^2 w_i - \gamma \sum_i z_i w_i g_i = \sum_i g_i$$

$$\beta \sum_i y_i w_i z_i + \alpha \sum_i g_i w_i z_i - \gamma \sum_i z_i^2 w_i = \sum_i z_i$$

The coefficients were evaluated from the available ^{Nat}Li and ^{12}C spectra, and the weights of the measured LiF spectrum. The equations were then solved by the LBL Source Library routine LINIT.

The parameter values obtained were

$$\alpha = 0.931 \pm 0.004 \ , \quad \beta = 0.0586 \pm 0.004 \ , \quad \gamma = 0.0709 \pm 0.004 \ .$$

The total number of events in the spectra were

^{Nat}Li	:	56,030
^{12}C	:	21,297
CF_2	:	30,198
LiF	:	31,007

Therefore the fraction of pions capturing on F in the LiF was

$$\frac{31{,}007 - \beta(56{,}030)}{31{,}007} = 0.894 \pm 0.007 \ .$$

The procedure was repeated with the roles of CF_2 and LiF, ^{12}C and ^{Nat}Li interchanged. The fraction of pions capturing on F in CF_2 was

found to be 0.822 ± 0.014. The resulting ^{19}F spectra obtained from Eqs. (E-1) and (E-2) did not differ significantly.